CHALMERS
UNIVERSITY OF TECHNOLOGY

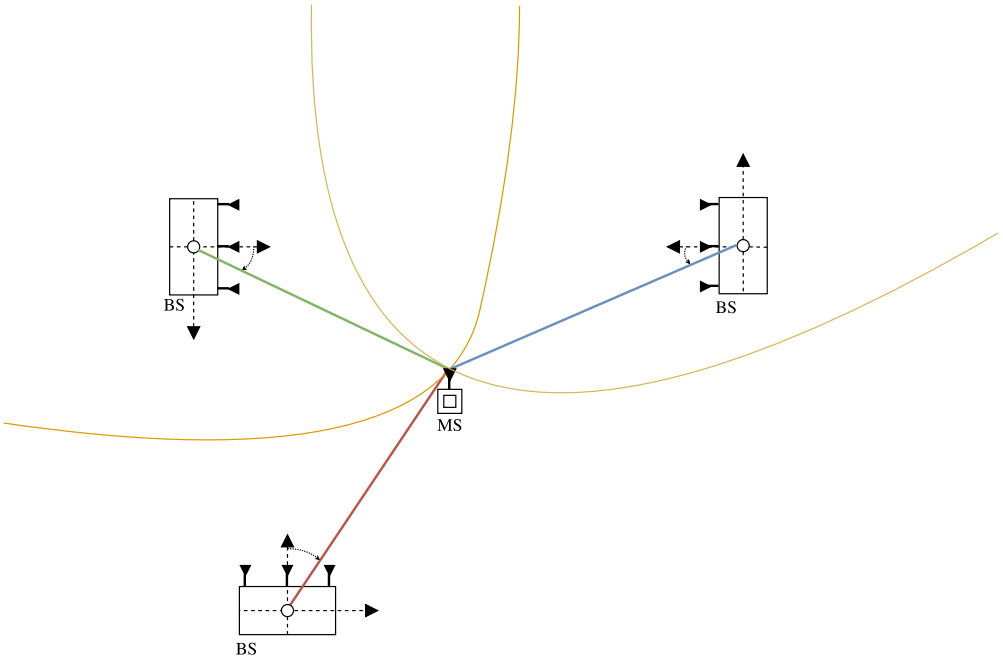

Millimeter-Wave Wideband Positioning with Multi-Antenna Transmitters and a Single-Antenna Receiver

A 5G Downlink Localization Approach with Synchronized Base Stations and Combined Angle and Time Measurements

Master's thesis in Master Programme Systems, Control and Mechatronics and Master Programme Communications Engineering

Philip Gertzell
Jacob Landelius

Department of Electrical Engineering
CHALMERS UNIVERSITY OF TECHNOLOGY
Gothenburg, Sweden 2020

Master's thesis 2020

Millimeter-Wave Wideband Positioning with Multi-Antenna Transmitters and a Single-Antenna Receiver

A 5G Downlink Localization Approach with Synchronized Base Stations and Combined Angle and Time Measurements

PHILIP GERTZELL
JACOB LANDELIUS

CHALMERS
UNIVERSITY OF TECHNOLOGY

Department of Electrical Engineering
Division of Communication systems
Cooperative systems
Chalmers University of Technology
Gothenburg, Sweden 2020

Millimeter-Wave Wideband Positioning with Multi-Antenna Transmitters and a Single-Antenna Receiver
A 5G Downlink Localization Approach with Synchronized Base Stations and Combined Angle and Time Measurements
PHIIP GERTZELL
JACOB LANDELIUS

Supervisors:
Henk Wymeersch, Chalmers University of Technology
Hanna Nyqvist, Aptiv
Examiner:
Henk Wymeersch, Chalmers University of Technology

Master's Thesis 2020
Department of Electrical Engineering
Division of Communication systems
Cooperative systems
Chalmers University of Technology
SE-412 96 Gothenburg
Telephone +46 31 772 1000

Cover: Illustration of the considered scenario, including three base stations in line-of-sight, see chapter 2.

Typeset in LaTeX
Gothenburg, Sweden 2020

Millimeter-Wave Wideband Positioning with Multi-Antenna Transmitters and a Single-Antenna Receiver
A 5G Downlink Localization approach with Synchronized Base Stations and combined Angle and Time Measurements
PHILIP GERTZELL
JACOB LANDELIUS
Department of Electrical Engineering
Chalmers University of Technology

Abstract

By the use of high frequency carrier signals (short waves), the robustness and accuracy of positioning in urban environments can be significantly improved compared to conventional Global Navigation Satellite Systems (GNSS), that relies on relatively long radio waves. A possible approach would be to utilize the 5G cellular network for localization. In this thesis we consider a Multiple-Input Single-Output (MISO) system operating with Millimeter-Wave (mmWave) carrier signals. Multiple base stations (BSs) are used to localize the position of a single mobile station (MS) in the Downlink (DL) channel. A two-step, low-complexity localization algorithm, combining Time-Difference-of-Arrival (TDOA) and Angle-of-Departure (AOD) measurements are exploited to estimate the unknown MS position. Theoretical lower bounds on localization accuracy are derived from an extensive Fisher information analysis. We propose an estimator that demonstrates cm-level accuracy as it attains the Cramér-Rao Lower Bound (CRLB) with improved positioning accuracy compared to TDOA-only and AOD-only estimators, even when bandwidth is limited or the transmit antennas are few.

Keywords: 5G, MISO, positioning, Millimeter-Wave, Time-Difference-of-Arrival, Angle-of-Departure, Fisher information, Cramér-Rao lower bound

Acknowledgements

We would like to thank Hanna Nyqvist, our supervisor at Aptiv for her expertise and excellent support. Other people we would like to express our gratitude to are Mohammad Hossein Moghaddam, Mats Björnerbäck, Alessio Fascista, Angelo Coluccia, Gonzalo Seco-Granados and especially Nil Garcia for guidance regarding technical issues. At last but not least, we want to thank Henk Wymeersch, our supervisor and examiner at Chalmers University of Technology for his support and patience regarding technical matters as well as his expertise and dedication for this thesis project.

Philip Gertzell and Jacob Landelius, Gothenburg, January 2020

Acronyms

4G Fourth Generation
5G Fifth Generation
ACC Adaptive Cruise Control
AD Autonomous Drive
ADAS Advanced Driver Assistance Systems
AEB Autonomous Emergency Breaking
AOA Angle-of-Arrival
AOD Angle-of-Departure
AWGN Additive White Gaussian Noise
BS base station
CP Cyclic Prefix
CRLB Cramér-Rao Lower Bound
D2D Device-to-Device
DL Downlink
EFIM Equivalent Fisher Information Matrix
FFT Fast Fourier Transform
FIM Fisher Information Matrix
GNSS Global Navigation Satellite Systems
GPS Global Positioning System
HD High-Definition
IFFT Inverse Fast Fourier Transform
ISI Intersymbol Interference
LOS Line-of-Sight
LS Least Squared
LTE Long Term Evolution
MC Monte-Carlo
MF Matched Filter
MIMO Multiple-Input Multiple-Output
MISO Multiple-Input Single-Output
ML Maximum Likelihood
MLE Maximum Likelihood Estimator
mmWave Millimeter-Wave
MS mobile station
NLLF Negative Log-Likelihood Function
NLOS Non-Line-of-Sight
NSD Noise Spectral Density
OFDM Orthogonal Frequency-Division Multiplexing

OLOS Obstructed-Line-of-Sight
PDF Probability Density Function
PEB Position Error Bound
PSD Power Spectral Density
RMSE Root-Mean-Square Error
SNR Signal-to-Noise Ratio
TDOA Time-Difference-of-Arrival
TOA Time-of-Arrival
TOF Time-of-Flight
UL Uplink
ULA Uniform Linear Array
URA Uniform Rectangular Array

Contents

Acronyms **ix**

1 Introduction **1**
1.1 Background . . . 1
1.2 Purpose . . . 2
1.3 Related Work . . . 3
1.4 Objective . . . 4
1.5 Limitations . . . 4
1.6 Ethics and Sustainability . . . 4

2 Theory of Radio Based Positioning **7**
2.1 System Model . . . 7
2.1.1 Transmitter Model . . . 7
2.1.2 Channel Model . . . 8
2.1.3 Receiver Model . . . 9
2.2 Fundamental Measurements for Radio Based Positioning . . . 10
2.2.1 Time Based Positioning Techniques . . . 11
2.2.1.1 Time of Arrival . . . 11
2.2.1.2 Time Difference of Arrival . . . 12
2.2.2 Angle Based Positioning . . . 13
2.2.2.1 Angle of Departure . . . 13
2.3 Performance Bounds . . . 14
2.3.1 Fisher Information . . . 15
2.3.1.1 Equivalent Fisher Information Matrix . . . 15
2.3.2 Cramér-Rao Lower Bound . . . 16
2.3.3 Position Error Bound . . . 16
2.4 Estimators . . . 17
2.4.1 Maximum Likelihood Estimation . . . 17
2.4.2 Estimation through Matched Filter . . . 17
2.4.3 Least Squares . . . 18
2.4.4 Error Metric: Root-Mean-Square Error . . . 19

3 Method **21**
3.1 Lower Bound on Channel Parameters . . . 22
3.1.1 FIM Derivation for Channel Parameters . . . 22
3.1.2 Cramér-Rao Lower Bound of Channel Parameters . . . 23

3.2 Lower Bound on Position 23
3.2.1 FIM Derivation for Position 23
3.2.2 Position Error Bound 25
3.3 Estimation of Position 25
3.3.1 Estimation of Channel Parameters with ML 25
3.3.2 Estimation of Position from Channel Estimates 27
3.4 Reference Scenario and Simulation Setup 28

4 Results and Analysis **31**
4.1 FIM Analysis 31
4.2 Channel and Position Estimations 33
4.2.1 Scenario 1: Estimates for Varying SNR 33
4.2.2 Scenario 2: Estimates for Varying Number of Antennas 37
4.2.3 Scenario 3: Estimates for Varying Bandwidth 38

5 Discussion **41**
5.1 Applications 41
5.2 Future Development 42

6 Conclusions **45**

Bibliography **47**

A Appendix A **I**

B Appendix B **III**

1
Introduction

This master thesis is a collaboration between Aptiv and Chalmers University of Technology and will investigate the possibility to apply Fifth Generation (5G) technology for host vehicle positioning. This is realized with mmWave carriers in a MISO setup, multiple synchronized BSs and a single-receiver antenna. A combination of time and angle measurements will be exploited to investigate if this setup can improve positioning accuracy in certain scenarios, compared to only using time or angle measurements.

In this chapter an introduction to the subject is presented as well as other related studies that have inspired throughout the project. The objective of this thesis is presented in more detail to give a better understanding of the main idea. Finally, ethical and environmental aspects are briefly discussed.

1.1 Background

Advanced Driver Assistance Systems (ADAS) is a rapidly growing industry with incitements from increasingly strict traffic regulations and safety assessments [1]. Mature ADAS features such as Autonomous Emergency Breaking (AEB), Adaptive Cruise Control (ACC) and lane centering [2] to name a few, constitutes the core of the future Autonomous Drive (AD) systems and has proven to decrease road accidents significantly [3]. AD is a forefront technology and is pushing the need of highly robust, accurate, computational and power efficient systems, one of them being vehicle positioning. A very common localization approach for AD and ADAS is by using various sensors such as radar, camera and LiDAR. These types of sensors provide local positioning and mapping of the surrounding environment of the host vehicle. For example, it can determine the position of surrounding vehicles and pedestrians relative to the host vehicle [4]. In order to build faulty-tolerant systems, redundancy is desirable to ensure safety functionality even if one system fails [5].

An important upcoming technology within AD is the real-time High-Definition (HD) map. A technology that can improve the current localization solutions with respect to the vehicle's environment and provide lane-level information beyond the reach of each individual in-vehicle sensors [6]. The key components in HD maps are precise global positioning and estimation of vehicular speed and direction. Furthermore, accurate and robust navigation systems and detailed real-time HD maps are important aspects for the development of fully autonomous vehicles.

In order to realize these visions a complement of today's dominant positioning techniques of GNSS must be found to create desired redundancy. GNSS positioning has achieved impressive accuracy (cm level) [7] in simple environments, such as open fields. However, high-precision GNSS systems are expensive and lack robustness and precision in complex environments, such as urban canyons, due to the nature of the relatively low carrier frequencies utilized by GNSS [8].

Another way of performing positioning is by the use of Fourth Generation (4G) technology, which is using radio waves close to the carrier frequencies of GNSS, single antenna and multiple BSs. This technique is used for example in emergency call positioning but have poor estimation accuracy (10-20 meters), it is therefore not a suitable solution for autonomous vehicles [7].

The current work on 5G technology is promising for future mobile communications, with important properties also beneficial for AD and ADAS. As a result of large carrier frequencies (small wavelengths), extended available bandwidths and large antenna arrays, 5G has the potential of precise positioning and mapping of the surrounding environment. The research is on-going and shows promising results. In [9], the possibilities to achieve accurate position estimations for a mmWave MISO system with one transmitting base station (BS) is investigated. The paper assumes a synchronized clock between the BS and the MS and can therefore solve the problem of MS position from TOA and AOD measurements. The estimators attain the CRLB with certain dimensional simplifications. Accurate position estimations for Multiple-Input Multiple-Output (MIMO) systems with Line-of-Sight (LOS), Non-Line-of-Sight (NLOS) and Obstructed-Line-of-Sight (OLOS) conditions are presented in [10].

Another important component in 5G is the Device-to-Device (D2D) communication which allows improved localization accuracy and increased coverage through cooperative positioning between mobile users [11]. The application of 5G in the automotive industry is not only of interest due to its positioning and mapping capabilities but also several other critical areas, for example intersection coordination optimization in vehicle-to-infrastructure scenarios [12].

With a growing 5G infrastructure and progressive research, it would be possible for the automotive industry to overcome the weaknesses of current positioning techniques.

1.2 Purpose

It is reasonable to assume that BSs in early phase 5G will have massive antenna arrays whereas mobile users will be limited to one antenna element due to the higher computational and power capabilities at stationary BSs. This makes it relevant to investigate localization with a single receiver antenna. The purpose of this thesis is to investigate the possibilities of using mmWaves in a MISO setup to determine a

stationary MS position with high accuracy (cm-level). Positioning in DL is considered in this work and is mainly motivated by the decreased computational burden at BSs and integrity protection of the user.

The thesis will also investigate how Fisher information can be used to derive appropriate estimator performance bounds and guide system design as well as enabling benchmarking for estimators.

1.3 Related Work

The general localization procedure in 4G and previous systems is by using TDOA measurements in either Uplink (UL) or DL [13, 14]. In DL-TDOA positioning the surrounding BSs are placed at known positions and transmit synchronized pilot signals which are picked up by the MS receiver as Time-of-Arrival (TOA) measurements. The position estimates comes from post-processing on the TDOA measurements at the MS by taking measurements from several BSs in relation to each other and by this rule out any asynchonization in the MS clock. The same estimation procedure is used for UL-TDOA localization but the measurements and parameter estimations are done at each individual BS.

Numerous promising results are found in the literature that present different MS position estimate techniques from a set of TDOA measurements. In [15] a closed-form localization algorithm is proposed to estimate the MS position. Additionally, several low complexity iterative approaches are found, for example [16, 17] that make use of TDOA-based positioning. To push the positioning accuracy further, the Long Term Evolution (LTE) standard has in its 9th release included a set of positioning reference signals which have been used to a large extend in [18, 19].

Several authors have investigated the possibility to combine time and angle measurements in order to increase the position estimation accuracy. In [20] a two-step Least Squared (LS) localization algorithm is proposed by combining TDOA and Angle-of-Arrival (AOA) measurements which proves to drastically increase the estimation performance compared to TDOA-only approaches. This study [21] also combine time and angle measurements to prove localization is possible with only two BSs instead of three, which is usually needed for TDOA-only.

With growing capabilities and system properties of the future 5G cellular networks with mmWave transmissions and MISO/MIMO systems, the possibilities of making use of the large antenna constellations seems interesting. In [22, 10], authors suggest that with the use of angular and time measurements, sub-meter positioning accuracy could be possible. Since AOA would contribute to an already busy UL channel and large antenna arrays in the early phase of 5G probably will be present only at the BSs, AOD would be a more interesting matter. Authors of [9] explore the use of AOD and TOA measurements and provide two novel estimation algorithms with reduced computational complexity. With AOD measurements the localization algorithms can be computed at the MS which utilizes the DL channel rather than the UL.

Furthermore, AOD provide localization possibilities in MIMO systems even with a single antenna in LOS [9].

1.4 Objective

The objective of this thesis is to create a 5G localization algorithm to position a MS, with only one receiver antenna, based on LOS DL pilot signals from multiple BSs. The estimation algorithm essentially has two tasks:

(i) To estimate channel parameters AOD and TDOA from each BS.
(ii) Based on estimated channel parameters from (i), estimate the MS position.

The Fisher information for the channel parameters will be computed and consequently the CRLB, the theoretical best performance bound, will be derived. Furthermore, the Fisher information for position will be derived from the channel Fisher Information Matrix (FIM) to evaluate the algorithm performance. An overview of the objective is illustrated in Fig. 1.1.

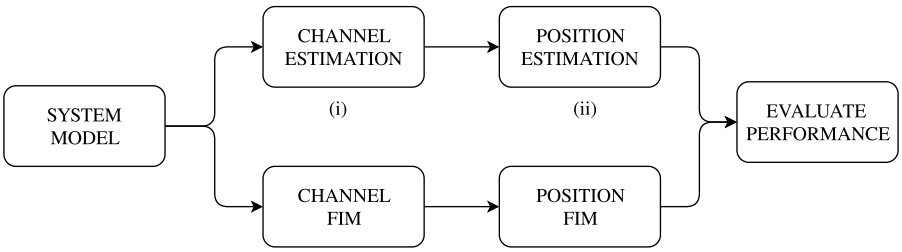

Figure 1.1: Overview illustration of the objective.

The algorithm is evaluated on simulated data from three types of scenarios: with different signal strengths, different available transmit antenna elements and for a variety of bandwidths. The position estimates will be evaluated by considering TDOA-only measurements, AOD-only measurements and a combination of both, presented in a comparison between all three scenarios. TDOA measurements are especially interesting in the case of few available antenna elements and AOD measurements when the bandwidth is restricted.

1.5 Limitations

A commonly used technique in localization is beamforming, which means that signals are sent in a concentrated direction to the target instead of an uniform sphere. In this thesis beamforming will not be included due to the restricted timeframe.

1.6 Ethics and Sustainability

Traffic related accidents kill 1.65 million people annually around the world [23] and is mainly due to human errors [24]. ADAS and the development of AD has proven

to reduce, and in the future almost eliminate the human factor during driving [3]. The development of high accuracy vehicle positioning methods is a crucial part of the engineering work towards AD and it is reasonable to believe it will significantly reduce traffic accidents.

With future AD technology the driving routes will be optimized which will lead to more efficient and safe driving, resulting in decreased emissions and power consumption [25].

Finally, localization services for users are likely to cause privacy concerns [26]. Computing localization in the UL demands an external agent of service, which could compromise user integrity. However, by performing localization in DL, which is investigated in this thesis, privacy and integrity of the user is easier to guarantee [27].

2

Theory of Radio Based Positioning

This chapter describes the theory which this thesis is based upon. In the following sections, a mathematical representation of the antennas and channel is presented as the system model. Followed by a theoretical account of radio-based positioning to give an in-depth understanding of the underlying concepts and techniques used in this thesis; including different measurement techniques, relevant estimators and theoretical performance bounds.

2.1 System Model

In this thesis a MISO Orthogonal Frequency-Division Multiplexing (OFDM) [28] system with total bandwidth $W_{\mathrm{B}} = 1/T_s$ is considered with T_s as the sample time. Furthermore N_{BS} perfectly synchronized[1] BSs is assumed, each BS with multiple transmitter antennas N_t. The two-dimensional position and orientation of each BS i is known and denoted $\mathbf{p}_i = [x_i \ y_i]^{\mathrm{T}} \in \mathbb{R}^2$. The unknown MS position is denoted $\mathbf{p} = [p_x \ p_y]^{\mathrm{T}}$ and has one antenna and an unknown clock bias b. As the estimates will be computed in the DL, the MS will be modelled as the receiver and the BSs as transmitters. The considered scenario setup is illustrated in Fig. 2.1.

2.1.1 Transmitter Model

The transmitter model is based on a Uniform Linear Array (ULA) structure thus only achieving two dimensional MS positioning (p_x, p_y) [29]. The carrier frequency f_c is in the upper spectral range of 5G ($>$ 24GHz) [30], with corresponding wavelength $\lambda_c = c/f_c$, where c is the known property of speed of light. Each BS sends G consecutive OFDM symbols, where the symbol on subcarrier $n \in \{0, \ldots, N-1\}$ during OFDM symbol $g \in \{0, \ldots, G-1\}$ is denoted by

$$\mathbf{s}_i^g[n] \in \mathbb{C}^{N_t \times 1} \quad i = 1, \ldots, N_{\mathrm{BS}}, \tag{2.1}$$

where $\mathbb{C}$ signify the complex signal domain. With $W_{\Delta \mathrm{B}} = W_{\mathrm{B}}/N$ as the spacing between each subcarrier . The symbols are converted from frequency domain into time domain by applying an Inverse Fast Fourier Transform (IFFT). A Cyclic Prefix (CP) is added to the signal in order to prevent Intersymbol Interference (ISI). The

[1] Synchronized means that every BS shares the same clock and sends out signals simultaneously, resulting in no clock bias between the BSs.

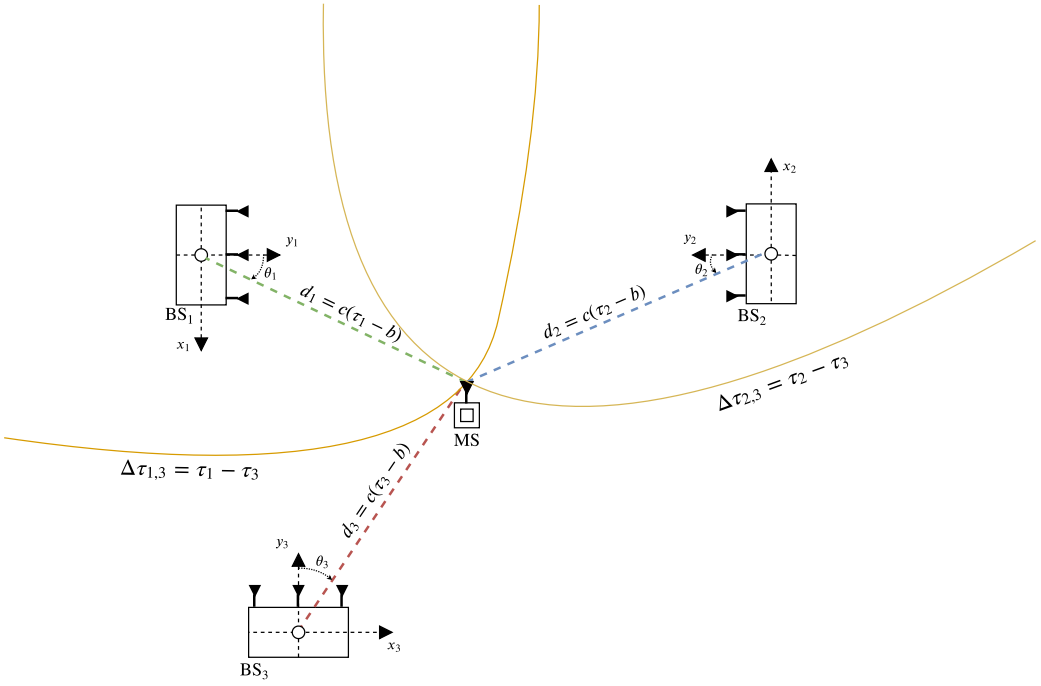

Figure 2.1: Geometry of the considered scenario.

length of CP is set to exceed the channel delay spread [2] [28] [31]. Furthermore, each antenna is assumed to be isotropic and transmitting with equal power, P_t.

2.1.2 Channel Model

The channel model is based on a typical urban environment with Additive White Gaussian Noise (AWGN) and assumed to have a dominant LOS path present from each BS to the MS. The channel vector is used to model the behaviour of each signal's propagation through the medium and its paths. It is assumed to be stationary during the G transmissions and the complex channel vector on subcarrier n from BS i to the MS is

$$\mathbf{h}_i^{\mathrm{T}}[n] = \gamma_i[n]\mathbf{a}_i^{\mathrm{H}}(\theta_i) \in \mathbb{C}^{N_t \times 1}. \tag{2.2}$$

Where $\mathbf{a}_i^{\mathrm{H}}(\theta)$ is the antenna steering vector of BS i and $\gamma_i[n]$ the complex channel gain on subcarrier n, expressed as

$$\gamma_i[n] = \alpha_i \exp\left(\frac{-j2\pi n\tau_i}{NT_s}\right). \tag{2.3}$$

Where τ_i is the measured TOF, expressed as

$$\tau_i = \|\mathbf{p} - \mathbf{p}_i\|/c + b, \tag{2.4}$$

[2] In a communication channel with multipath propagation, ISI can occur due to subsequent symbols interfering with each other. ISI can be prevented by adding a CP before the transmitted symbol with a length equal to the length of the longest multipath, defined from the delay spread.

where $\|\cdot\|$ denotes the norm. Furthermore, $\alpha_i = e^{j\phi_i}/\rho_i$ is the channel path loss with

$$\rho_i = (4\pi d_i/\lambda_c)\,. \tag{2.5}$$

Here, ϕ_i is a uniformly distributed random variable between $[0, 2\pi]$. The distance from the MS to a BS is expressed as $d_i = \|\mathbf{p} - \mathbf{p}_i\|$. The transmitter response vector describes how phase angles of each subcarrier at each antenna are affected depending on their AOD [32] and can initially be modeled as

$$\mathbf{a}_i\left(\theta_i\right) = \begin{bmatrix} 1 \\ e^{-j\frac{2\pi}{\lambda_n} d_\lambda \sin(\theta_\mathrm{i})} \\ \vdots \\ e^{-j(N_t-1)\frac{2\pi}{\lambda_n} d_\lambda \sin(\theta_i)} \end{bmatrix} \in \mathbb{C}^{N_t \times 1}. \tag{2.6}$$

The subcarrier wavelength is defined as $\lambda_n = c/(n/NT_s + f_c)$ but since $f_c >> W_\mathrm{B}$ is full-filled, the channel is considered to follow narrowband characteristics and can be simplified to $\lambda_n \approx \lambda_c$ [31]. The distance between each antenna element is expressed as $d_\lambda = \lambda_c/2$. Thus, the antenna response vector from (2.6) can be simplified to

$$\mathbf{a}_i(\theta_i) = \begin{bmatrix} 1 \\ e^{-j\pi \sin(\theta_i)} \\ \vdots \\ e^{-j(N_t-1)\pi \sin(\theta_i)} \end{bmatrix} \in \mathbb{C}^{N_t \times 1}, \tag{2.7}$$

where the AOD to the corresponding BS is defined as

$$\theta_i = \operatorname{atan2}\left(p_y - y_i, p_x - x_i\right) \tag{2.8}$$

and $\operatorname{atan2}\left(y, x\right)$ is the four-quadrant inverse tangent. There will be no significant contribution to the channel model equation from the receiver antenna since its response vector is modelled as a scalar with value 1.

2.1.3 Receiver Model

The receiver is considered stationary, composed of one antenna element and an unknown clock bias b with respect to the synchronized BSs. To generate the received signal $\mathbf{Y}_i$ the CP is first removed and further processed through a Fast Fourier Transform (FFT), the received signal at the g-th transmission with subcarrier n is modeled as

$$y_i^g[n] = \sqrt{P_t}\mathbf{h}_i^\mathrm{T}[n]\mathbf{s}_i^g[n] + \omega_i^g[n], \tag{2.9}$$

where $\omega_i^g[n]$ is AWGN with zero mean and the variance σ^2 and P_t is the transmitted power per antenna. All the observations from BS i are stored into the matrix

$$\mathbf{Y}_i = \begin{bmatrix} y_i^0[0] & \cdots & y_i^{G-1}[0] \\ \vdots & \ddots & \vdots \\ y_i^0[N-1] & \cdots & y_i^{G-1}[N-1] \end{bmatrix}. \tag{2.10}$$

Note that the g-th column of $\mathbf{Y}_i$ can be expressed as

$$\mathbf{y}_i^g = \sqrt{P_t}\alpha_i\tilde{\boldsymbol{\gamma}}_i(\tau_i) \odot \left(\mathbf{a}_i^{\mathrm{H}}(\theta_i)\mathbf{S}_i^g\right)^{\mathrm{T}} + \boldsymbol{\omega}_i^g, \tag{2.11}$$

where $\odot$ is the element-wise vector multiplication. The complex channel gain is no longer expressed in terms of α_i

$$[\tilde{\boldsymbol{\gamma}}(\tau_i)]_n = \exp(-j2\pi n\tau_i/(NT_s)), \forall n = 0, \ldots, N-1 \tag{2.12}$$

and with the symbols as

$$\mathbf{S}_i^g = [\boldsymbol{s}_i^g[0] \ldots \boldsymbol{s}_i^g[N-1]] \in \mathbb{C}^{N_t \times N}. \tag{2.13}$$

At this point it is worth to notice that the received signal model consist of four unknown parameters, TOA τ_i, AOD, θ_i, noise variance σ^2 and complex gain α_i. In order to resolve the MS position these parameters needs to be estimated, as will further be described in chapter 3.

The theoretical received Signal-to-Noise Ratio (SNR) is defined in dB as

$$\mathrm{SNR}_i = 10\log_{10}\left(\frac{N_t P_t \left|\alpha_i\right|^2}{N_0 W_{\mathrm{B}}}\right) \tag{2.14}$$

where $10\log_{10}(\cdot)$ denotes the base-10 logarithm. The noise variance of the received signal is

$$\sigma^2 = N_0 W_{\mathrm{B}} = T_0 k_{\mathrm{B}} W_{\mathrm{B}} \tag{2.15}$$

where T_0 is the thermal noise temperature, expressed as the standard room temperature in Kelvin, and k_{B} is the Boltzmann constant. The observed SNR for each transmission is measured by

$$\mathrm{SNR}_i = \frac{\mathbb{E}[(|\mathbf{y}_i^g|)^2 - \mathrm{var}(\boldsymbol{\omega}^g)]}{\mathrm{var}(\boldsymbol{\omega}^g)} \tag{2.16}$$

where $\mathbb{E}(\cdot)$ denotes the expected value and $\mathrm{var}(\cdot)$ denotes the variance.

2.2 Fundamental Measurements for Radio Based Positioning

One important aspect in positioning with radio waves is signal measurements. Different types of measurements are preferable in different scenarios to achieve accurate positioning estimates due to possible constraints and simplifications. Typical measurements of time and angles give unique information regarding the unknown position. Combining these types of measurements give additional information and could result in better positioning estimates. When the localization procedure is performed at the MS it is regarded as DL positioning and for UL the computations are performed at the BSs [33].

2.2.1 Time Based Positioning Techniques

By relying on signal strength and phase of the received signals the travel time of the signals can be measured. Since radio waves propagates through air with the speed of light, even a relatively small error in time would result in drastically inaccurate estimations. The margin of error on these measurements must therefore be very low. Common issues to deal with are asynchronous BSs and individual clock biases of all MSs. Thus, even a small internal clock error could result in major estimated distance error. An additional disadvantage with this type of measurement is in the case of no clear LOS path for the propagated signal, which may result in scattering and diffraction. In the case of NLOS and no present LOS, time measurements are delayed which results in inaccurate time estimates. This issue can be solved if the path is resolvable, meaning that the receiver is capable of determine the path of the signal [33].

2.2.1.1 Time of Arrival

The TOA measurement is commonly used in many traditional positioning systems such as GNSS [34]. It corresponds to the Time-of-Flight (TOF) of radio waves from a transmitter at time τ to a receiver at time $\tau + (d/c)$, where d is the distance from the transmitter to the receiver and c is the known property of speed of light.

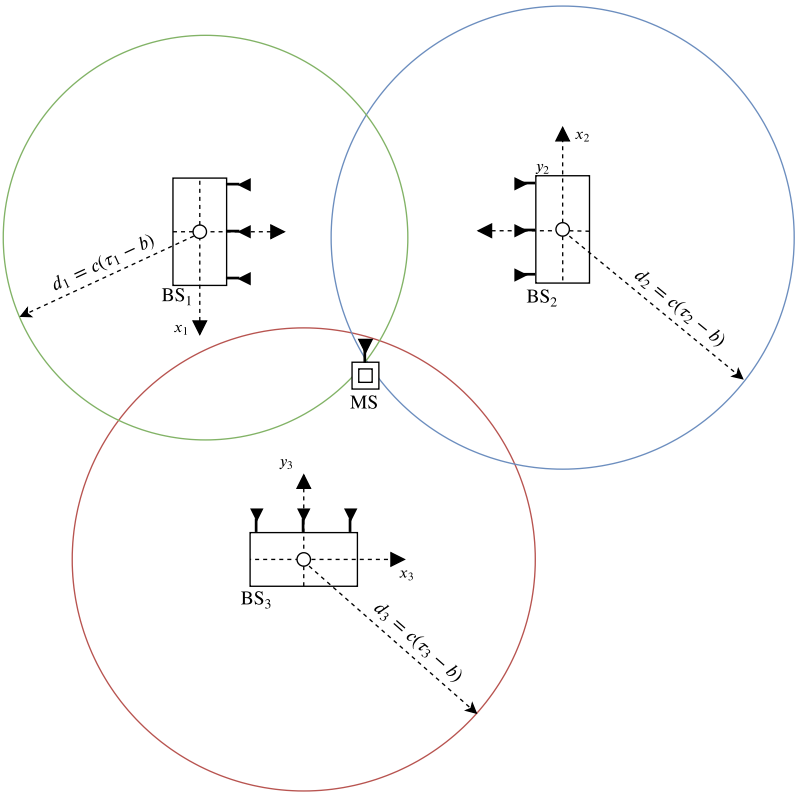

Figure 2.2: Illustration of the concept of TOA.

The time estimation in the clock of the receiver with multiple BS present is expressed as

$$\hat{\tau}_i = \frac{d_i}{c} + b + \omega_i, \quad i = 1, \ldots, N_{\text{BS}} \tag{2.17}$$

where b is the clock bias between the supposedly asynchronous transmitter and receiver, ω_i is measurement noise and N_{BS} is the number of BSs [33]. Based on the time estimates, the distances between the BSs and the MS can be derived as

$$\hat{d}_i = c(\hat{\tau}_i - b). \tag{2.18}$$

When only considering time measurements a circular positioning restriction will be realized, i.e. the time estimation gives the distance to a receiver but not the direction, resulting in a circle with its origin at the transmitter with radius d_i as illustrated in Fig. 2.2. A distance cannot be correctly estimated with clock bias present with TOA measurement and a removal action of the clock bias needs to be performed. This measurement technique can on the other hand be realised with a minimum of two BS present, with the assumption of a fully synchronized system.

2.2.1.2 Time Difference of Arrival

One way to solve the TOA bias issue is by taking measurements from multiple synchronized BSs and relate the different measurements with measurements from a chosen reference station. Further advantages with the TDOA approach is that the time of the transmitted signal can be unknown, since only the TOA is needed in order to remove the clock bias [3]. A TDOA measurement is expressed as

$$\Delta\hat{\tau}_i = \hat{\tau}_i - \hat{\tau}_j, \quad i \neq j \tag{2.19}$$

where $\hat{\tau}_i$ is the TOA as expressed in (2.17) and $\hat{\tau}_j$ the TOA for a chosen reference station j. With the use of time difference, the clock bias b at the receiver is cancelled out, with the assumption of perfectly synchronized BSs. Note that the measurement noise for each TOA measurement is randomly distributed and therefore cannot be cancelled out in the same way as the bias [33].

The time difference can then be related to distances in the same manner as (2.17) by calculating the distance difference from the reference station to all other BSs to the MS. These differences of distance have an infinite number of solutions and result in hyperbolas when related over different distance relation ratios between the reference station and the BSs. With multiple BSs transmitting signals, an area with some uncertainty can be found through multilateration [35], as illustrated in Fig. 2.3. The TDOA measurement basically consists of several TOA measurements which are represented as circles in the two-dimensional plane with different biases. The intersection of two of those TOA circles from different BSs indicates a potential estimate and several circle intersections construct the hyperbola. From this it follows that a minimum of three BSs are needed to realise this time-based measurement.

[3] Given that the BSs are synchronized to the same clock.

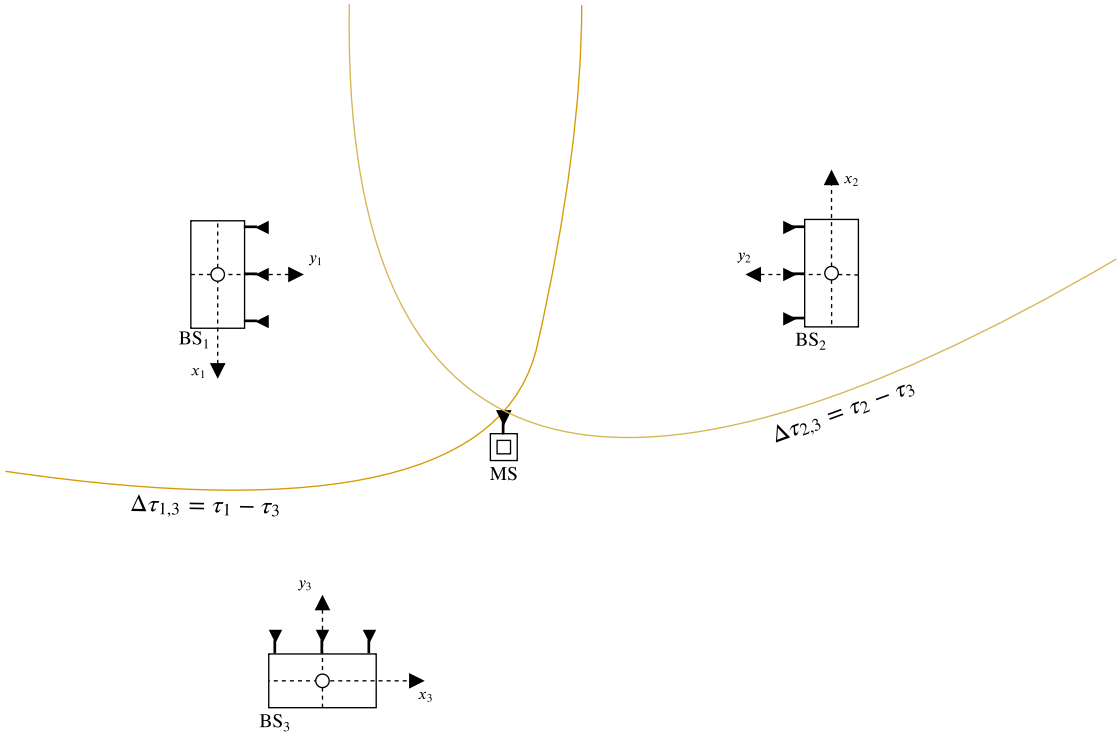

Figure 2.3: Illustration of the concept of TDOA.

Worth mentioning is that the estimator performance is dependent on the chosen reference BS and should be investigated in each individual case in order to assure the best possible performance.

2.2.2 Angle Based Positioning

This measuring technique uses angles of the transmitted signal departures or the received signal's arrival angles. These type of measurements gives information regarding the direction of the transmission signal or the direction from which a signal is received, resulting in a straight line from the transmitter to the receiver. Multiple antennas, such as different types of antenna arrays, must be present at either the transmitter or receiver in order to obtain the corresponding angle measurements. Usually the orientation of the transmitter in DL and orientation of receiver in UL must also be known to interpret these measurements correctly. Note that a single-antenna receiver is considered in this thesis, therefore only the direction of the transmitted signal can be realised. Both the azimuth and elevation angles can be measured, the azimuth determines the direction and the elevation the height. Unless multiple BSs are considered, angled based measurements alone cannot be used to estimate the MS position and is usually combined with time measurements [36].

2.2.2.1 Angle of Departure

AOD is the angle of which a signal is transmitted with from the transmitter antenna. Assuming that the orientation of the transmitter antenna structure is known, these

measurements can be realized. The estimated position is found where the signal departure directions intersects, represented as straight lines in Fig. 2.4.

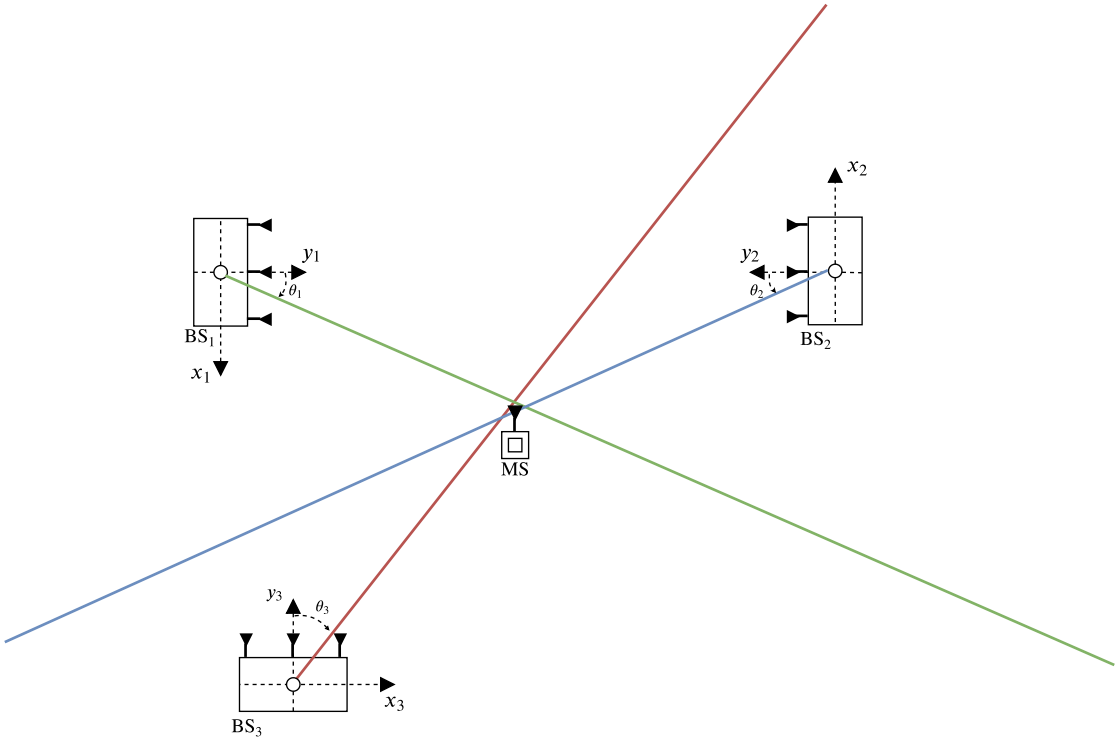

Figure 2.4: Illustration of the concept of AOD.

A received signal y_k at time $\tau + \delta\tau$, transmitted from a ULA antenna structure at time τ can be expressed as

$$y_k = \mathbf{a}^{\mathrm{T}}(\theta_k)s(\tau + \delta\tau) + \omega, \quad k = 1, \ldots, K. \tag{2.20}$$

Where θ_k is the unknown departure angle, s the transmitted signals, ω some measurement noise and K are the total number of paths. The antenna response vector for the transmitter is expressed as

$$\mathbf{a}(\theta_k) = \exp \frac{j2\pi d_\delta \sin\theta_k}{\lambda} \tag{2.21}$$

where d_δ is the spacing between the antenna elements and λ is the signal wavelength [29]. The interpretation of the antenna response vector is a way to represent the relative signal phase rotation of each antenna element. The AOD measurement is possible with the presence of multiple transmit antennas. However, in order to determine the user position it must be combined with either time based measurements or by considering two or more BSs [36].

2.3 Performance Bounds

When evaluating the performance of a constructed estimator it is beneficial to relate it to some theoretical performance bound. In estimation theory CRLB is the

theoretical lowest variance an unbiased estimator can achieve. It is common to state this performance bound, which can be derived from the Fisher information.

2.3.1 Fisher Information

In a system where a set of observed random variables $\mathbf{Y}$ depends on an unknown parameter vector $\boldsymbol{\zeta}$, the Fisher information can be used to measure how much information the observation $\mathbf{Y}$ carries about the unknown $\boldsymbol{\zeta}$. The Fisher information can be interpreted as the curvature of a high dimensional space of a log function [37].

The Fisher information can be derived from the law of total probability through the second derivative of the logarithm of the Probability Density Function (PDF) [38]. The multi-variable FIM is expressed as

$$\mathbf{I}(\boldsymbol{\zeta}) = -\mathbb{E}\left[\frac{\partial^2 \log f(\mathbf{Y}|\boldsymbol{\zeta})}{\partial \boldsymbol{\zeta} \partial \boldsymbol{\zeta}^{\mathrm{T}}}\right] \tag{2.22}$$

where $f(\cdot)$ is the PDF. The FIM is a positive semi-definite square matrix, i.e. $\mathbf{b}^{\mathrm{T}}\mathbf{I}\mathbf{b} \geq 0$ for any arbitrary vector $\mathbf{b}$. Considering $\hat{\boldsymbol{\zeta}}$ as an unbiased estimator of $\boldsymbol{\zeta}$ the expression of the FIM is well-known to be related to the estimation error covariance matrix the following way [39]

$$\mathbb{E}\left[(\boldsymbol{\zeta} - \hat{\boldsymbol{\zeta}})(\boldsymbol{\zeta} - \hat{\boldsymbol{\zeta}})^{\mathrm{T}}\right] \succeq \mathbf{I}(\boldsymbol{\zeta})^{-1}. \tag{2.23}$$

A FIM with large eigenvalues values contains much information about the unknown and will result in a covariance matrix with low eigenvalues. A diagonal FIM implies no or very low correlation in the parameter vector.

When AWGN is present on the measurements the equation for the FIM can be simplified into the following [40]

$$\mathbf{I}(\boldsymbol{\zeta}) = \Re\{\nabla_{\boldsymbol{\zeta}} \mathbf{m}^{\mathrm{H}}(\boldsymbol{\zeta}) \boldsymbol{\Sigma}^{-1} \nabla_{\boldsymbol{\zeta}} \mathbf{m}(\boldsymbol{\zeta})\} \tag{2.24}$$

where $\mathbf{m}(\boldsymbol{\zeta})$ is the mean value of the observation $\mathbf{Y} = \mathbf{m}(\boldsymbol{\zeta}) + \omega$, with $\omega \sim \mathcal{CN}(0, \boldsymbol{\Sigma})$, i.e. the noise-free observation. Here, $\boldsymbol{\Sigma}$ is the covariance matrix of the complex measurement noise and $\nabla_{\boldsymbol{\zeta}}$ represent the gradient with respect to the unknown parameter vector $\boldsymbol{\zeta}$.

2.3.1.1 Equivalent Fisher Information Matrix

It is common for a system to have multiple unknown parameters but there might only be a few of interest and the rest are considered as nuisance parameters that needs to be considered but which values are not of importance. The Equivalent Fisher Information Matrix (EFIM) is a way to express the information in terms of a certain set of parameters that are considered known and is found through the Shurs complement [41].

Consider two sets of unknown parameter vectors $\mathbf{z}_1$ and $\mathbf{z}_2$. In order to determine the theoretical best performance with restricted knowledge of parameter $\mathbf{z}_2$ the EFIM is derived. The FIM in (2.22) can be expressed in matrix form and broken up as

$$\mathbf{I}(\mathbf{z}_1, \mathbf{z}_2) = \begin{bmatrix} \mathbf{A}(\mathbf{z_1}) & \mathbf{B}(\mathbf{z_1}, \mathbf{z_2}) \\ \mathbf{B}^{\mathrm{T}}(\mathbf{z_1}, \mathbf{z_2}) & \mathbf{C}(\mathbf{z_2}) \end{bmatrix}. \tag{2.25}$$

The EFIM of unknown parameter $\mathbf{z}_2$ is obtained by inverting (2.25), extracting the submatrix corresponding to $\mathbf{z}_2$ and then inverting the resulting matrix. The result is mathematically described as

$$\mathbf{I}^{\mathrm{E}}(\mathbf{z}_2) = \mathbf{C}(\mathbf{z_2}) - \mathbf{B}^{\mathrm{T}}(\mathbf{z_1}, \mathbf{z_2})\mathbf{A}(\mathbf{z_1})^{-1}\mathbf{B}(\mathbf{z_1}, \mathbf{z_2}). \tag{2.26}$$

The EFIM with respect to $\mathbf{z}_2$ will give the information of $\mathbf{z}_2$ considering $\mathbf{z}_1$ unknown and will take any cross-correlation terms between $\mathbf{z}_1$ and $\mathbf{z}_2$ into account.

2.3.2 Cramér-Rao Lower Bound

The CRLB is a common bound for benchmarking estimators as it describes the best theoretical performance an unbiased estimator can achieve and is tightly related to the FIM. This bound is convenient during performance evaluation of estimators because if an estimator reaches the CRLB it has the optimal accuracy performance [39]. The CRLB gives the lowest possible covariance values of an unbiased estimator $\hat{\boldsymbol{\zeta}}$ of the parameter vector $\boldsymbol{\zeta}$ as in (2.23), where the CRLB is the inverse of $\mathbf{I}(\boldsymbol{\zeta})$

$$\mathrm{CRLB}_j = \left[\mathbf{I}(\boldsymbol{\zeta})^{-1}\right]_j \tag{2.27}$$

and $[\cdot]_j$ denotes the diagonal entry. In order to relate CRLB to the estimation errors metric, described in subsection 2.4.4, it is commonly expressed as a standard deviation, derived from the square root of the desired individual diagonal entry j.

$$\sigma_{\mathrm{CRLB}}(j) = \sqrt{\mathrm{CRLB}(j)}. \tag{2.28}$$

2.3.3 Position Error Bound

In order to evaluate the theoretical best positions possible for a certain scenario the Position Error Bound (PEB) can be used. It is a common way in localization to express the standard deviation of the joint of the x- and y-coordinates. It is based on the FIM described in (2.22) and expressed as

$$\mathrm{PEB} = \sqrt{\mathrm{tr}\left\{[\mathbf{I}(\boldsymbol{\zeta})^{-1}]_{i,j}\right\}} \tag{2.29}$$

where $\boldsymbol{\zeta}$ is an unknown position parameter vector, $[\cdot]_{i,j}$ denotes the row and column which usually corresponds to the position coordinates (x, y) and $\mathrm{tr}\{.\}$ denotes the matrix trace.

2.4 Estimators

In this section common estimators used for radio based localization are presented. Their advantages and disadvantages are highlighted regarding optimality and computational complexity. Finally, an error metric is presented for performance evaluation.

2.4.1 Maximum Likelihood Estimation

The Maximum Likelihood Estimator (MLE) is used to estimate parameter values of an observation model that tries to mimic a certain observation. The MLE maximizes the probability that measurements are from a certain sample space. In other words the Maximum Likelihood (ML) finds the most likely parameters to realize the observation. In order to analytically solve the maximization problem the likelihood function L needs to be differentiable w.r.t. the parameters. The ML is defined as

$$\hat{\mathbf{x}} = \arg\max_{\mathbf{x}\in\mathcal{X}} L(\mathbf{x};\mathbf{Y}) \tag{2.30}$$

where $\mathcal{X} = \left\{\mathbf{x} : \mathbf{x} \in \mathbb{R}^k\right\}$ is the parameter space of $\mathbf{x}$, $L(\mathbf{x};\mathbf{Y}) = f(\mathbf{Y}|\mathbf{x})$, where $f(\cdot)$ is the PDF and $\mathbf{Y}$ is the observation matrix [42]. This results in a k-dimensional parameter search to obtain the values of $\mathbf{x}$ to maximize (2.30). For convenience it is common to maximize over the natural logarithm of the likelihood function $l(\mathbf{x};\mathbf{Y}) = \log L(\mathbf{x};\mathbf{Y})$. Therefore (2.30) can be rewritten as the maximum log-likelihood the following way

$$\hat{\mathbf{x}} = \arg\max_{\mathbf{x}\in\mathcal{X}} l(\mathbf{x};\mathbf{Y}) \tag{2.31}$$

The MLE becomes optimal and efficient for infinite number of samples which means that it is unbiased, reaches the CRLB and has the lowest Root-Mean-Square Error (RMSE) compared to any other estimator. ML is therefore also consistent for sufficient large sample sizes which means that the estimated parameter will match the true parameter value [39].

The computational complexity of ML is high due to the large sample sizes needed for efficiency and also depends on the size of the parameter vector $\mathbf{x}$. The complexity order increases with the parameter size as $\mathcal{O}(Q^k)$ with Q being the sample size.

2.4.2 Estimation through Matched Filter

For a known deterministic signal and an additive independent white noise process with the Noise Spectral Density (NSD)[4] $N_0/2$, a Matched Filter (MF) is capable of filter out as much of the noise as possible while still retaining the known signal [43]. In order to derive the MF, consider a known deterministic signal $x[t]$ passed through an AWGN channel, so that the received signal is $r[t] = x[t] + w[t]$, where $w[t]$ is

[4]The NSD is the Power Spectral Density (PSD) of thermal noise containing equal power for all frequencies.

noise with spectral density $N_0/2$. In order to reproduce the transmitted signal $x[t]$ and reduce the amount of noise as much as possible, it is desirable to process the received signal through a filter such that the output of the filter can be expressed as

$$y[t] = \sum_{\tau=-\infty}^{\infty} h[\tau]x[t-\tau] + h[\tau]w[t-\tau]. \tag{2.32}$$

The MF seeks a solution that maximizes the SNR of the output from this process at time $t = \tau$. From (2.32) and from the fact that the NSD is $N_0/2$, the SNR is expressed as

$$\text{SNR} = \frac{2}{N_0} \frac{\sum_{\tau=-\infty}^{\infty} |h[\tau]x[t-\tau]|^2}{\sum_{\tau=-\infty}^{\infty} h^2[\tau]} \tag{2.33}$$

In order to find $h[\tau]$ that maximizes the SNR, (2.33) can be simplified by using Schwarz's inequality [43]. The inequality is thus formulated as

$$\text{SNR} \leq \frac{2}{N_0} \frac{\sum_{\tau=-\infty}^{\infty} |h[\tau]|^2 \sum_{\tau=-\infty}^{\infty} |x[t-\tau]|^2}{\sum_{\tau=-\infty}^{\infty} h^2[\tau]} \tag{2.34}$$

$$= \frac{2}{N_0} \sum_{\tau=-\infty}^{\infty} |x[t-\tau]|^2 = \frac{2}{N_0} \sum_{\tau=-\infty}^{\infty} |x[t]|^2 = \frac{2E_x}{N_0}, \tag{2.35}$$

where E_x is the energy spectral density of the transmitted signal. This shows that the SNR of the process output is maximized when $h[\tau] = x[t-\tau]$, finally expressed in the frequency domain [43] as

$$H(f) = X^*(f)e^{-j2\pi f\tau}. \tag{2.36}$$

In signal processing, a MF can be used when measured signals contain known signal templates with unknown parameters. To illustrate this, consider a signal $x[t]$, transmitted through a AWGN with an unknown delay τ such that the received signal can be expressed as $y[t] = x[t-\tau] + w[t]$. The unknown time delay can be estimated by creating a one-dimensional search for all possible values of τ

$$\hat{\tau} = \arg\max_{\tau} \sum_{\tau=-\infty}^{\infty} |X^*(f)e^{-j2\pi f\tau}Y(f)|^2. \tag{2.37}$$

The ideal match filter in this case is $H(f) = X^*(f)e^{-j2\pi f\tau}$, and the maximized MF $\tilde{H}(f) = X^*(f)e^{-j2\pi f\hat{\tau}}$.

2.4.3 Least Squares

The LS estimation method is a special case of ML when the distribution of the additive noise process is zero-mean Gaussian. In LS the cost function corresponds

to the sum of squared differences between a model and an observation. The value of the model parameter vector is estimated by minimizing this cost function w.r.t. the parameters. The linear LS algorithm finds a trend in the Gaussian distributed data that has the least error distances to the data points. The estimator is commonly used for over-determined systems where more equations are available than unknown parameters. The LS is expressed as

$$\hat{\mathbf{x}} = \arg\min_{\mathbf{x}\in\mathcal{X}} \frac{1}{2}\|\boldsymbol{\psi} - f(\mathbf{x})\|^2_{\boldsymbol{\Sigma}^{-1}} \tag{2.38}$$

which is equivalent to

$$\hat{\mathbf{x}} = \arg\min_{\mathbf{x}\in\mathcal{X}} (\boldsymbol{\psi} - f(\mathbf{x}))^{\mathrm{T}}\boldsymbol{\Sigma}^{-1}(\boldsymbol{\psi} - f(\mathbf{x})) \tag{2.39}$$

where $\mathcal{X} = \left\{\mathbf{x} : \mathbf{x} \in \mathbb{R}^k\right\}$ is the parameter space, $\boldsymbol{\psi}$ is the observation, $f(\cdot)$ is the model and a common way to weight the impact of each parameter in $\mathbf{x}$ is to choose $\boldsymbol{\Sigma}^{-1}$ as the inverse of the covariance matrix of $\boldsymbol{\psi}$ [39].

The solution to the LS problem can be found where the gradient of the cost function is zero, which yields an analytical solution for linear LS. In general, an analytical solution for the non-linear LS can not be guaranteed and a numerical solution must therefore be found. The linear LS estimator with additive and zero mean noise is unbiased, but this is not generally true for non-linear LS estimators [39].

2.4.4 Error Metric: Root-Mean-Square Error

In order to evaluate the performance of an estimator common practice is to calculate the RMSE which is the square root of the expected value of the squared error, the difference between an observation and a true parameter value. For an estimate $\hat{\mathbf{x}}$, of a parameter vector $\mathbf{x}$, the resulting RMSE is the standard deviation of the estimation errors and is expressed as

$$\mathrm{RMSE}(\hat{\mathbf{x}}) = \sqrt{\mathbb{E}\left\{(\hat{\mathbf{x}} - \bar{\mathbf{x}})^2\right\}} = \sqrt{\frac{\sum_{j=1}^{U}(\hat{\mathbf{x}}_j - \bar{\mathbf{x}})^2}{U}} \tag{2.40}$$

where $\bar{\mathbf{x}}$ is the true parameter value and U is the sample size. The metric is sensitive to outliers due to the mean calculation.

3
Method

The setup in this chapter is based on the objective presented in section 1.4 and the system model in section 2.1. With this into account, the FIM and CRLB of the channel parameters are derived for each BS. A transformation of the channel FIM is done to derive the expression of the position FIM and ultimately the PEB. Furthermore, estimators for the channel parameters are developed and finally a position estimator is presented. This chapter further includes a detailed description of the considered reference scenario and the intended simulation setups. An elaborated overview of the method of this thesis is presented in Fig 3.1.

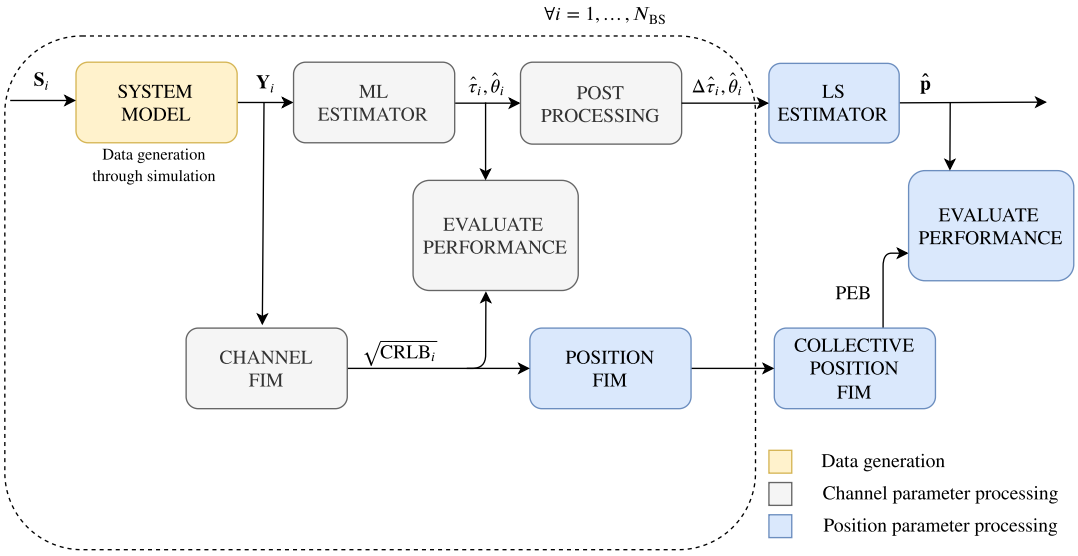

Figure 3.1: Flowchart of the thesis method, including estimation algorithms, theoretical bounds and performance evaluation.

From the simulated observations $\mathbf{Y}_i$ channel estimates TOA τ_i and AOD θ_i are found using the ML estimator. The performance of these estimates were evaluated in a comparison between theoretical lowest standard deviation, derived from the channel FIM. In order to remove the MS clock bias post-processing was done and TDOA calculated. This procedure was done N_{BS} times before feeding the information into the LS estimator that, together with information from the channel FIM, provide the final MS position estimates $\hat{\mathbf{p}}$. The position FIM was derived from all channel FIMs and further derived into the PEB which was used to evaluate the performance of the position estimates.

3.1 Lower Bound on Channel Parameters

In order to benchmark the implemented estimators, theoretical performance bounds was calculated for each scenario. The CRLB is the theoretical lowest variance an unbiased estimator can have and it is an efficient way to determine the estimators sufficiency. In this section the FIM for the channel parameters is calculated and then further CRLB is derived from the FIM.

3.1.1 FIM Derivation for Channel Parameters

The observation equation (2.9) from section 2.1 can be seen as a noise-free observation for the g-th transmission over the n-th subcarrier and was rewritten the following way

$$m_i^g[n] = \sqrt{P_t}\alpha_i e^{-j\frac{2\pi n\tau_i}{NT_s}}\mathbf{a}_i^{\mathrm{H}}(\theta)\mathbf{s}_i^g[n] \quad i = 1, \ldots, N_{\mathrm{BS}}. \tag{3.1}$$

The unknown channel parameter vector was defined as $\boldsymbol{\zeta}_i = [\rho_i, \phi_i, \tau_i, \theta_i]^{\mathrm{T}}$ and $\hat{\boldsymbol{\zeta}}_i$ was considered an unbiased estimator of $\boldsymbol{\zeta}_i$. The expression of the channel FIM is generally known to be related to the estimation error covariance matrix as described in (2.23) from chapter 2

$$\mathbb{E}\left[(\boldsymbol{\zeta}_i - \hat{\boldsymbol{\zeta}}_i)(\boldsymbol{\zeta}_i - \hat{\boldsymbol{\zeta}}_i)^{\mathrm{T}}\right] \succeq \mathbf{I}_{\boldsymbol{\zeta}_i}^{-1} \tag{3.2}$$

where the FIM for the channel parameters was expressed as $\mathbf{I}_{\boldsymbol{\zeta}_i}$. The definition of the FIM was declared in (2.22) but since AWGN is assumed, (2.22) is simplified according to (2.24) as

$$\mathbf{I}_{\boldsymbol{\zeta}_i} = \frac{2}{\sigma^2}\sum_{g=0}^{G-1}\sum_{n=0}^{N-1}\Re\left\{\nabla_{\boldsymbol{\zeta}}^{\mathrm{H}} m_i^g[n]\nabla_{\boldsymbol{\zeta}} m_i^g[n]\right\} \tag{3.3}$$

where $\Re\{\cdot\}$ denotes the real-part operator and with the gradient of the noise-free observations with respect to $\boldsymbol{\zeta}_i$ as

$$\nabla_{\boldsymbol{\zeta}} m_i^g = \begin{bmatrix} \partial m_i^g/\partial\rho_i & \partial m_i^g/\partial\phi_i & \partial m_i^g/\partial\tau_i & \partial m_i^g/\partial\theta_i \end{bmatrix}^{\mathrm{T}} \tag{3.4}$$

which when calculated yields

$$\nabla_{\boldsymbol{\zeta}} m_i^g[n] = e^{j\left(\phi - \frac{2\pi n\tau_i}{NT_s}\right)}\begin{bmatrix} \mathbf{a}_i^{\mathrm{H}}(\theta_i)\mathbf{s}_i^g[n] \\ j\rho_i\mathbf{a}_i^{\mathrm{H}}(\theta_i)\mathbf{s}_i^g[n] \\ \frac{-j2\pi n}{NT_s}\rho_i\mathbf{a}_i^{\mathrm{H}}(\theta_i)\mathbf{s}_i^g[n] \\ -j\pi\cos\theta_i\rho_i\mathbf{a}_i^{\mathrm{H}}(\theta_i)\mathbf{D}\mathbf{s}_i^g[n] \end{bmatrix} \tag{3.5}$$

where $\mathbf{D} = \mathrm{diag}[0, \ldots, N_t - 1]$ is a $[N_t \times N_t]$ matrix with the antenna indices on the diagonal. The variance σ^2 was chosen as the noise spectral density defined in (2.15). The result is a 4×4 matrix $\mathbf{I}_{\boldsymbol{\zeta}_i}$. In order to verify its validity, common matrix operations were performed to ensure matrix full-rank. According to [9],

which have a similar setup, unique pilot signals needs to be transmitted over all antennas. Furthermore, at least two transmissions and one subcarrier or at least two subcarriers and one transmission, as well as unique signals from all antennas, is required to ensure non-singularity.

3.1.2 Cramér-Rao Lower Bound of Channel Parameters

In accordance to (2.27) and (2.28) in subsection 2.3.2 the lower bounded standard deviation for each channel parameter can be achieved by taking the square root of each individual diagonal entry of the inverted FIM, $\mathbf{I}_{\boldsymbol{\zeta}_i}$, from (3.3).

$$\sqrt{\text{CRLB}_j} = \sqrt{\left[\mathbf{I}_{\boldsymbol{\zeta}_i}^{-1}\right]_j}. \tag{3.6}$$

Appropriate scenario parameters such as number of transmit antennas, number of subcarriers, can be found by minimizing the CRLB, as the bound gives the lowest possible error standard deviations. By performing this analysis, proper parameters can be determined before any estimation algorithms are introduced which guides the system design and indicates what estimators that would be appropriate for a given scenario. More on this in section 4.1.

3.2 Lower Bound on Position

In order to derive the FIM for position, a transformation from the channel parameters needs to be performed. Since the BSs and the MS are not synchronized, a clock bias will be present in the relation between the channel parameters and the positions. The asynchronization issue can be solved by considering measurements from multiple BSs.

3.2.1 FIM Derivation for Position

A transformation needs to be performed from the channel parameters to position parameters. From the channel FIM $\mathbf{I}_{\boldsymbol{\zeta}_i}$ a Jacobian transformation was applied to obtain the FIM of the unknown position parameter vector

$$\boldsymbol{\eta}_i = \left[\rho_i, \phi_i, \mathbf{p}^{\mathrm{T}}, b\right]^{\mathrm{T}} \in \mathbb{C}^{5\times 1} \tag{3.7}$$

as

$$\mathbf{I}_{\boldsymbol{\eta}_i} = \mathbf{T}_i^{\mathrm{T}} \mathbf{I}_{\boldsymbol{\zeta}_i} \mathbf{T}_i, \tag{3.8}$$

where the transformation matrix between the channel parameters and position parameters was defined as the partial derivatives of the channel parameter vector $\boldsymbol{\zeta}_i$ with respect to the position parameter vector $\boldsymbol{\eta}_i$

$$\mathbf{T}_i \overset{\text{def}}{=} \frac{\partial \boldsymbol{\zeta}_i^{\mathrm{T}}}{\partial \boldsymbol{\eta}_i} = \begin{bmatrix} \partial\rho_i/\partial\rho_i & \partial\rho_i/\partial\phi_i & \partial\rho_i/\partial\mathbf{p} & \partial\rho_i/\partial b \\ \partial\phi_i/\partial\rho_i & \partial\phi_i/\partial\phi_i & \partial\phi_i/\partial\mathbf{p} & \partial\phi_i/\partial b \\ \partial\tau_i/\partial\rho_i & \partial\tau_i/\partial\phi_i & \partial\tau_i/\partial\mathbf{p} & \partial\tau_i/\partial b \\ \partial\theta_i/\partial\rho_i & \partial\theta_i/\partial\phi_i & \partial\theta_i/\partial\mathbf{p} & \partial\theta_i/\partial b \end{bmatrix} = \begin{bmatrix} 1 & 0 & \mathbf{0} & 0 \\ 0 & 1 & \mathbf{0} & 0 \\ 0 & 0 & \partial\tau_i/\partial\mathbf{p} & \partial\tau_i/\partial b \\ 0 & 0 & \partial\theta_i/\partial\mathbf{p} & \partial\theta_i/\partial b \end{bmatrix}. \tag{3.9}$$

By recalling that only τ_i (2.4) and θ_i (2.8) are geometric functions of $\mathbf{p}$, the corresponding derivatives was found as

$$\partial\tau_i/\partial\mathbf{p} = \frac{1}{c}\Big[\cos(\theta_i), \sin(\theta_i)\Big]^{\mathrm{T}} \tag{3.10}$$

$$\partial\theta_i/\partial\mathbf{p} = \frac{1}{\|\mathbf{p}-\mathbf{p}_i\|}\Big[-\sin(\theta_i), \cos(\theta_i)\Big]^{\mathrm{T}} \tag{3.11}$$

$$\partial\theta_i/\partial b = 0, \qquad \partial\tau_i/\partial b = 1 \tag{3.12}$$

and the rest of the entries are zero as they do not depend on any parameter in the position parameter vector in (3.7). The physical relations between time and position was defined in (2.4) from section 2.1 and between angle and position in (2.8).

The transformation results in a 5×5 always singular matrix $\mathbf{I}_{\boldsymbol{\eta}_i}$. The matrix singularity was expected as the clock bias that was introduced in the transformation is unknown. In order to deal with the singularity, a collective FIM was constructed consisting of the individual FIM for all BSs. Since the position elements in the matrix provides information for each BS, the position and bias related elements are summed together, while the nuisance parameters are independent of each other and are therefore providing unique information. For convenient reasons the collective position FIM $\mathbf{I}_{\boldsymbol{\eta}_i}$ was broken up as

$$\mathbf{I}_{\boldsymbol{\eta}_i} = \begin{bmatrix} \mathbf{A}_i & \mathbf{B}_i \\ \mathbf{B}_i^{\mathrm{T}} & \mathbf{C}_i \end{bmatrix}, \tag{3.13}$$

where $\mathbf{A}_i \in \mathbb{R}^{2\times2}$, $\mathbf{B}_i \in \mathbb{R}^{3\times2}$, and $\mathbf{C}_i \in \mathbb{R}^{3\times3}$. The collective position FIM, of the parameter vector $\boldsymbol{\eta}$ of length $2N_{\mathrm{BS}} + 3$ expressed as

$$\boldsymbol{\eta} = [\rho_1, \phi_1, \ldots, \rho_{N_{\mathrm{BS}}}, \phi_{N_{\mathrm{BS}}}, \mathbf{p}^{\mathrm{T}}, b]^{\mathrm{T}} \tag{3.14}$$

is of the form

$$\mathbf{I}_{\boldsymbol{\eta}} = \begin{bmatrix} \mathbf{A}_1 & & & \mathbf{B}_1 \\ & \ddots & & \vdots \\ & & \mathbf{A}_{N_{\mathrm{BS}}} & \mathbf{B}_{N_{\mathrm{BS}}} \\ \mathbf{B}_1^{\mathrm{T}} & \cdots & \mathbf{B}_{N_{\mathrm{BS}}}^{\mathrm{T}} & \sum_{i=1}^{N_{\mathrm{BS}}} \mathbf{C}_i \end{bmatrix}. \tag{3.15}$$

Note that, for $N_{\mathrm{BS}} \neq 1$ the empty entries in (3.15) are equal to zero. The nuisance parameters are of no special interest in this thesis and the EFIM was therefore

calculated, defined as (2.26). The EFIM with respect to position and bias $\boldsymbol{\pi} = [\mathbf{p}^{\mathrm{T}}, b]^{\mathrm{T}}$ was calculated as

$$\mathbf{I}_{\boldsymbol{\pi}}^{\mathrm{E}} = \sum_{i=1}^{N_{\mathrm{BS}}} \mathbf{C}_i - \sum_{i=1}^{N_{\mathrm{BS}}} \mathbf{B}_i^{\mathrm{T}} \mathbf{A}_i^{-1} \mathbf{B}_i. \tag{3.16}$$

In order to do a complete theoretical performance assessment, as described in section 1.4, the FIM for position needs to be calculated when only considering TOA measurements as well as when only considering AOD measurements. The calculations are done with the same reasoning as above, for detailed calculations see Appendix A.

3.2.2 Position Error Bound

The PEB defined in (2.29), with the diagonal entries of the inverse of (3.16) give a collective position bound that was used as the theoretical assessment of achievable performance

$$\mathrm{PEB} = \sqrt{\mathrm{tr}\left\{ [\mathbf{I}_{\boldsymbol{\pi}}^{\mathrm{E}}]_{1:2,1:2}^{-1} \right\}}. \tag{3.17}$$

3.3 Estimation of Position

In this section, a channel estimator is proposed to estimate the AOD and TOA from each BS. The approach makes use of a two-dimensional parameter space MLE. This section also includes an in-depth description of combining the local estimates to obtain the global MS position by solving a weighted LS problem. The true TOA cannot be estimated from the received signal as it comes with an unknown clock bias. However, an estimation of TOA and its clock bias is possible.

3.3.1 Estimation of Channel Parameters with ML

The ML approach, as defined in subsection 2.4.1 was derived in order to estimate the channel parameters TOA τ_i and AOD θ_i. The MLE is a suitable choice as the received signal $\mathbf{y}_i^g \in \mathbb{C}^{N \times 1}$ can be modeled as a complex Gaussian distribution such that

$$\mathbf{y}_i^g \sim \mathcal{CN}(\alpha_i \tilde{\mathbf{h}}_i^g(\boldsymbol{\kappa}_i), \sigma^2), \tag{3.18}$$

with $\tilde{\mathbf{h}}^g(\boldsymbol{\kappa}_i)$ based on (2.11), defined as

$$\tilde{\mathbf{h}}_i^g(\boldsymbol{\kappa}_i) = \tilde{\boldsymbol{\gamma}}_i(\tau_i) \odot \left(\mathbf{a}_i^{\mathrm{H}}(\theta_i) \mathbf{S}_i^g \right)^{\mathrm{T}}. \tag{3.19}$$

Defining $\boldsymbol{\kappa}_i = [\tau_i,\ \theta_i]^{\mathrm{T}}$ and recalling from (2.12) that $\tilde{\boldsymbol{\gamma}}_i(\tau_i) = \exp(-j2\pi n \tau_i / (NT_s))$, the estimated channel parameter vector $\hat{\boldsymbol{\kappa}}_i$ were found from the MLE, expressed as

$$\hat{\boldsymbol{\kappa}}_i = \arg\max_{\boldsymbol{\kappa}_i} \left[\max_{\alpha_i, \sigma^2} L_i(\boldsymbol{\kappa}_i, \alpha_i, \sigma^2) \right]. \tag{3.20}$$

With $L(\boldsymbol{\kappa}_i, \alpha_i, \sigma^2|\mathbf{Y}_i) = f(\mathbf{Y}_i|(\boldsymbol{\kappa}_i, \alpha_i, \sigma^2)$ defined as the likelihood function and $f(\cdot)$ is the PDF of the received signal $\mathbf{y}_i^g$. From the definition of the general complex Gaussian distribution model [44] and (3.18), L_i can be expanded as

$$L(\boldsymbol{\kappa}_i, \alpha_i, \sigma^2|\mathbf{Y}_i) = \prod_{g=0}^{G-1} \frac{1}{2\pi\sigma^2} \exp\left(\frac{\left\| \mathbf{y}_i^g - \alpha_i \tilde{\mathbf{h}}_i^g(\boldsymbol{\kappa}_i) \right\|^2}{-2\sigma^2} \right). \tag{3.21}$$

By applying the natural logarithm of (3.21) and exploiting the fact that the expression is invariant of σ, the PDF gets proportional to the Negative Log-Likelihood Function (NLLF), expressed as

$$l(\boldsymbol{\kappa}_i, \alpha_i|\mathbf{Y}_i) = \sum_{g=0}^{G-1} \left\| \mathbf{y}_i^g - \alpha_i \tilde{\mathbf{h}}_i^g(\boldsymbol{\kappa}_i) \right\|^2. \tag{3.22}$$

The MLE of τ_i and θ_i in (3.20) can now be compressed and expressed as a minimization problem

$$\hat{\boldsymbol{\kappa}}_i = \arg\min_{\boldsymbol{\kappa}_i} \left[\min_{\alpha_i} l_i(\boldsymbol{\kappa}_i, \alpha_i|\mathbf{Y}_i) \right]. \tag{3.23}$$

Through derivation of (3.22) in (3.23) w.r.t to α_i, a minimized expression of α_i is found as a function of τ_i and θ_i, the estimation can thus be expressed as

$$\hat{\alpha}_i(\boldsymbol{\kappa}_i) = \frac{\sum_{g=1}^{G} (\tilde{\mathbf{h}}_i^g)^{\mathrm{H}}(\boldsymbol{\kappa}_i) \mathbf{y}_i^g}{\sum_{g=1}^{G} \left\| (\tilde{\mathbf{h}}_i^g)^{\mathrm{H}}(\boldsymbol{\kappa}_i) \right\|} \tag{3.24}$$

The MLE (3.23) can together with (3.24) finally form a matched filter

$$\hat{\boldsymbol{\kappa}}_i = \arg\min_{\boldsymbol{\kappa}_i} \sum_{g=0}^{G} \left\| \mathbf{y}_i^g - \hat{\alpha}_i(\boldsymbol{\kappa}_i) \tilde{\mathbf{h}}_i^g(\boldsymbol{\kappa}_i) \right\|^2. \tag{3.25}$$

A low-complexity two-dimensional grid search was implemented in order to solve the minimization problem, with iterative grid refinement. The estimator holds a relatively high computational complexity because of its order of $\mathcal{O}(Q^2)$. Where Q is recalled as the number of iterations per grid search vector, which needs to be coherent with the CRLB to reach the theoretical lower bound.

In order to reduce the computational complexity, a two-step estimation procedure was performed. First, a low resolution grid search was performed, to single out a rough indication of the minimum. The search distance was limited from 0 to

150 meters and the angular search grid from $-\pi/2$ to $\pi/2$ radians. From this initial estimate, a refined grid search with incremented resolution, determined by the CRLB, was performed on the limited search area to estimate the global minimum. The performance of the algorithm was evaluated by running the estimator over $U = 500$ Monte-Carlo (MC) simulations and calculating the RMSE as defined in (2.40)

$$\mathrm{RMSE}_i(\hat{\boldsymbol{\kappa}}_i) = \sqrt{\frac{\sum_{j=1}^{U}(\hat{\boldsymbol{\kappa}}_{i,j} - \bar{\boldsymbol{\kappa}}_i)^2}{U}}, \tag{3.26}$$

where $\bar{\boldsymbol{\kappa}}_i$ is the vector of ground truth values for τ_i and θ_i.

3.3.2 Estimation of Position from Channel Estimates

Since a clock bias is present due to the MS asynchronous clock, a removal action was performed as the TOA estimates were post-processed and TDOA calculated as

$$\Delta\hat{\tau}_i = \hat{\tau}_i - \hat{\tau}_{N_{\mathrm{BS}}}, i \neq N_{\mathrm{BS}} \tag{3.27}$$

where the reference BS was chosen as $i = N_{\mathrm{BS}}$. A short remark, the noise-free TDOA $\Delta\tau_i = (d_i - d_{N_{\mathrm{BS}}})/c$, is not dependent on the clock bias b. An observation vector was constructed as

$$\hat{\boldsymbol{\psi}} = [\Delta\hat{\tau}_1, \ldots, \Delta\hat{\tau}_{N_{\mathrm{BS}}-1}, \hat{\theta}_1, \ldots, \hat{\theta}_{N_{\mathrm{BS}}}]^{\mathrm{T}} \in \mathbb{R}^{(2N_{\mathrm{BS}}-1)\times 1}. \tag{3.28}$$

Note that the number of TDOA measurement is $N_{\mathrm{BS}} - 1$ and therefore less than the number of TOA measurements. Since the TDOA and AOD are geometric functions of $\mathbf{p}$ (2.4) (2.8), the noise-free relation can be written as $\boldsymbol{\psi} = f(\mathbf{p})$

$$f(\mathbf{p}) = \begin{bmatrix} \Delta\hat{\tau}_1(\mathbf{p}) \\ \vdots \\ \Delta\hat{\tau}_{N_{\mathrm{BS}}-1}(\mathbf{p}) \\ \hat{\theta}_1(\mathbf{p}) \\ \vdots \\ \hat{\theta}_{N_{\mathrm{BS}}}(\mathbf{p}) \end{bmatrix} = \begin{bmatrix} \frac{1}{c}\left(\|\mathbf{p} - \mathbf{p}_1\| - \|\mathbf{p} - \mathbf{p}_{N_{BS}}\|\right) \\ \vdots \\ \frac{1}{c}\left(\|\mathbf{p} - \mathbf{p}_{N_{\mathrm{BS}}-1}\| - \|\mathbf{p} - \mathbf{p}_{N_{BS}}\|\right) \\ \operatorname{atan2}\left(p_y - y_1, p_x - x_1\right) \\ \vdots \\ \operatorname{atan2}\left(p_y - y_{N_{\mathrm{BS}}}, p_x - x_{N_{\mathrm{BS}}}\right) \end{bmatrix} \in \mathbb{R}^{(2N_{\mathrm{BS}}-1)\times 1}. \tag{3.29}$$

This over-determined system then immediately lead to the following weighted least squares problem as defined in (2.39)

$$\hat{\mathbf{p}} = \arg\min_{\mathbf{p}} (\hat{\boldsymbol{\psi}} - f(\mathbf{p}))^{\mathrm{T}} \boldsymbol{\Sigma}^{-1} (\hat{\boldsymbol{\psi}} - f(\mathbf{p})). \tag{3.30}$$

The weighting matrix $\boldsymbol{\Sigma}^{-1}$ was found from the inverse of the covariance matrix, calculated as the covariance of the post-processed channel estimates $\hat{\boldsymbol{\psi}}$ over $U = 500$ MC simulations. Note that the transformation function (3.29) from channel parameters to position is non-linear, the resulting LS is therefore non-linear which do not guarantee unbiased estimations, as concluded in subsection 2.4.3.

In order to realize a complete comparison between the estimator presented above and when using only TDOA measurements and only AOD measurements, the LS was formulated in a similar manner as above for these restricted estimators, see Appendix B.

The LS problem was solved with a two-dimensional search over different MS positions. It was implemented by first exploiting the AOD estimations from (3.25) which provides a limited search area where the N_{BS} bearing lines intersects. In the case of accurate AOD estimations, this algorithm will effectively reduce the computational complexity, while poor AOD estimations might result in a search grid which is out of bounds of the true values. In such a case a regular two-dimensional search was performed. Similar as with the MLE in subsection 3.3.1, by using the information gained from the position FIM a theoretical sufficient step-size can dynamically be found during simulation. This provided the needed accuracy, without any extended tuning to accomplish the theoretical bounds. The resolution of the search was hence determined by the PEB.

Finally, in order to evaluate the position estimator performance the RMSE (2.40) was calculated as

$$\text{RMSE}(\hat{\mathbf{p}}) = \sqrt{\frac{\sum_{j=1}^{U}(\hat{\mathbf{p}}_j - \mathbf{p})^2}{U}}. \tag{3.31}$$

3.4 Reference Scenario and Simulation Setup

In this section the considered reference scenarios are described which are based on the fundamental system model as described in section 2.1 and will pin point the system parameters that lay the foundation of three different simulation setups.

A static MS is considered in all three scenarios with the distance from the MS to all BSs set constant to approximately 30m. The relative AOD from all BSs to the MS is approximately 35°. The orientation and global position of the BSs are considered known and placed in the Cartesian reference system:

$$\begin{aligned}\mathbf{p}_1 &= [-30, -5]^{\text{T}}\ [\text{m}]\\ \mathbf{p}_2 &= [5, -30]^{\text{T}}\ [\text{m}]\\ \mathbf{p}_3 &= [30, 5]^{\text{T}}\ [\text{m}].\end{aligned}$$

The location of the MS is known at $\mathbf{p} = [0, 0]^{\text{T}}$ [m]. All three BSs transmit three sequential OFDM signals $G = 3$, where the maximum number of antenna elements N_t of each BS is limited to 80 without any beamforming. The transmit power is varied such that the observed SNR $\leq$ 15dB, recall the definition of SNR (2.16) described in section 2.1. The carrier frequency is f_c = 24GHz and the maximum available bandwidth $W_{\text{B}} \leq$ 700MHz divided on $N = 40$ subcarriers with the sampling time

$T_s = 1/W_{\mathrm{B}}$. The bias of the asynchronous receiver clock $b = 20$[ns]. A complete set of reference scenario parameters are found in Table 3.1.

Table 3.1: Table of reference scenario parameters.

Parameter name	**Notation**	**Value**	**Unit**
Bandwidth	W_{B}	≤ 700	[MHz]
Carrier frequency	f_c	24	[GHz]
Signal-to-noise ratio	SNR	≤ 15	[dB]
Clock bias	b	20	[ns]
Number of BSs	N_{BS}	3	[-]
Number of antennas	N_t	≤ 80	[-]
Number of subcarriers	N	40	[-]
Number of transmissions	G	3	[-]

In order to evaluate the system performance, three variations of the system setup are considered:

Scenario 1) Varied SNR from -10dB to 15dB with antennas fixed to $N_t = 40$ and bandwidth set to $W_{\mathrm{B}} = 100$MHz

Scenario 2) Number of transmit antennas N_t is varied from 2 to 80 with SNR fixed to 5dB and bandwidth set to $W_{\mathrm{B}} = 100$MHz

Scenario 3) Bandwidth W_{B} is varied from 10 to 700 MHz with 40 transmit antennas and SNR fixed at 5dB.

The intention of Scenario 1 is to investigate the estimator performance for different signal strengths and the minimum required SNR. In Scenario 2 information from angular measurements are expected to be insufficient when antenna elements are few, but increase when they are many. TDOA measurements is expected to be eminent for any number of antennas as the bandwidth is still high. With low available bandwidth, as investigated in Scenario 3, TDOA measurements are expected to be inadequate, while AOD measurements alone are expected to provide necessary information as a large antenna array is utilized. The main purpose is to investigate if the combination of TDOA and AOD measurements provide more accurate position estimations than TDOA-only or AOD-only estimators.

To measure the performance of the estimators the metric RMSE is used and evaluated in relation to the theoretical CRLB and PEB of the corresponding scenario. For each simulation point 500 MC simulations are performed. Note that the distance and AOD from each BS to the MS are the same, the channel estimation simulations can therefore be combined into one plot and thus reaching 1500 MC simulations instead of 500. In the case of estimators not reaching the CRLB or PEB the distribution of the errors is computed and presented in the shape of a histogram in order to pinpoint the cause, for example with bias present or if the variance of the distribution is deviant from the CRLB.

4
Results and Analysis

This chapter presents the obtained results of the FIM analysis for the channel and position as well as the performance of the proposed estimators in the specified scenarios, presented in section 3.4. The estimators are evaluated in relation to the theoretical lower bounds of CRLB and PEB, derived from the respective FIM.

4.1 FIM Analysis

In this section the results of the channel and position FIM are presented and analyzed. Moreover, CRLB and PEB are derived from the respective FIM and presented for different values of number of antennas N_t and bandwidth W_{B}. In Fig. 4.1 the theoretical lowest standard deviation is shown, i.e. the $\sqrt{\mathrm{CRLB}(\cdot)}$ for channel parameters TOA τ and AOD θ. SNR is set constant at 5dB and when varying antennas and the bandwidth is constant at 100MHz. When varying the bandwidth, the number of antennas is set to 40. As observed, TOA (top left) is not effected by the increase of antennas while AOD (top right) have a significant decrease in standard deviation as the number of antenna elements grow larger. The opposite behaviour is observed when varying the bandwidth, proving a strong relation between TOA and bandwidth and between AOD and antenna elements. Note that the AOD accuracy stagnates as the number of antennas reach 80 and the same for TOA with bandwidths above 800MHz. Moreover, this provides information regarding parameter selection and what parameter values contribute to additional accuracy.

The same behaviour as for the channel parameters is observed in Fig. 4.2 when translated to positions. The combined time and angle PEB shows great potential for accurate positioning, especially between 10 to 40 antenna elements and between 100 and 400MHz of bandwidth.

By analyzing the FIM the relation between different measurements and system parameters are found and indicates that TOA measurements will provide important information for very few antennas and significantly increase estimation accuracy when the bandwidth is increased. AOD measurements on the other hand show promising results in scenarios even when bandwidth is restricted and provides significant information as the number of antenna elements increases. The combination of both angle and time measurements have potential to always provide more or equally much information, especially at the transition between few and many antenna elements and between low and high bandwidths.

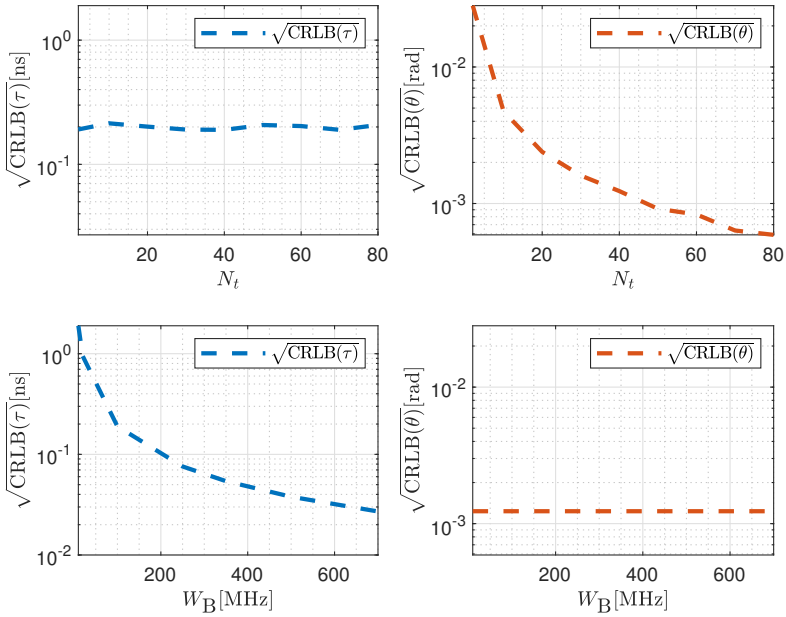

Figure 4.1: The channel FIM represented as $\sqrt{\text{CRLB}(\cdot)}$ (3.6) for different number of antennas (top) and bandwidths (bottom).

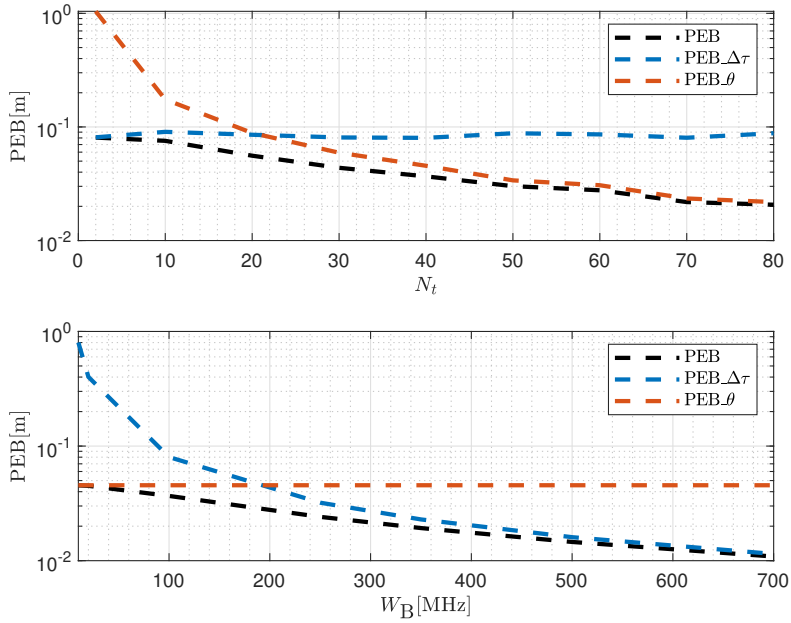

Figure 4.2: The position FIM represented as PEB (3.17) for different number of antennas (top) and bandwidths (bottom).

4.2 Channel and Position Estimations

In this section the simulation results from the different scenarios, as described in section 3.4 are presented and compared to their corresponding theoretical lower bounds. From simulations for the channel estimations it is found that the MLE successfully reaches the bounds in all scenarios.

The two-step refinement estimation approach, proposed in subsection 3.3.1 is illustrated in Fig. 4.3. The first course grid search is capable of providing a rough estimate for the channel parameters and from the information provided by this search, a refined estimation is achieved in the second search.

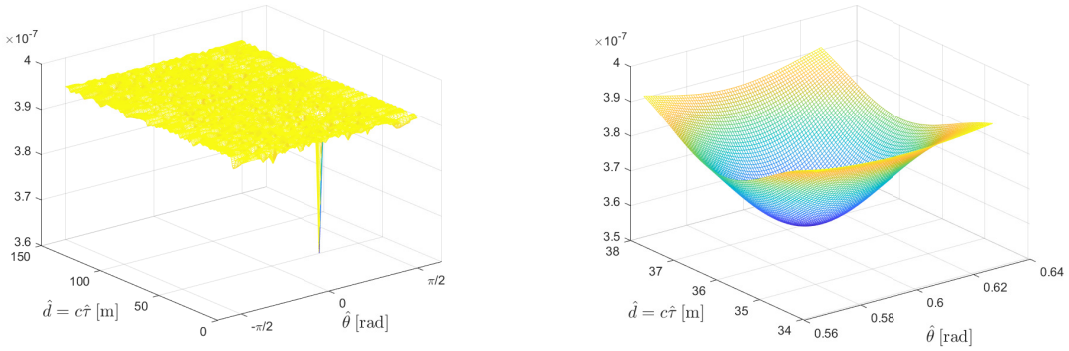

(a) Course grid over a large search area.

(b) Refined grid over a restricted search area.

Figure 4.3: ML estimation of channel parameters in two steps. The first estimate (a) gives a rough estimation of the channel parameters. Based on the first estimates a refined grid search (b) is computed with an iterative grid refinement.

4.2.1 Scenario 1: Estimates for Varying SNR

Evaluation results of the channel RMSEs from all BSs compared to the corresponding CRLBs for varying SNRs are presented in Fig. 4.4 and a combination of all three BSs channel simulations in Fig. 4.5 (a). The numerical results with two significant figures are presented in Table 4.1. As observed, the estimator successfully attains the CRLBs from -5dB and up, but fails to do so when the SNR is less than -5dB. Results show that for very low SNR (< -5dB) the estimator can still perform well during some simulations and in other cases completely fail to estimate the parameters, considered as outliers [1]. This is an expected behaviour since estimators generally rarely achieve the CRLB at these SNRs [45].

[1] Estimates are regarded as outliers if the resulting position estimate deviates more than 3 meters from the true position.

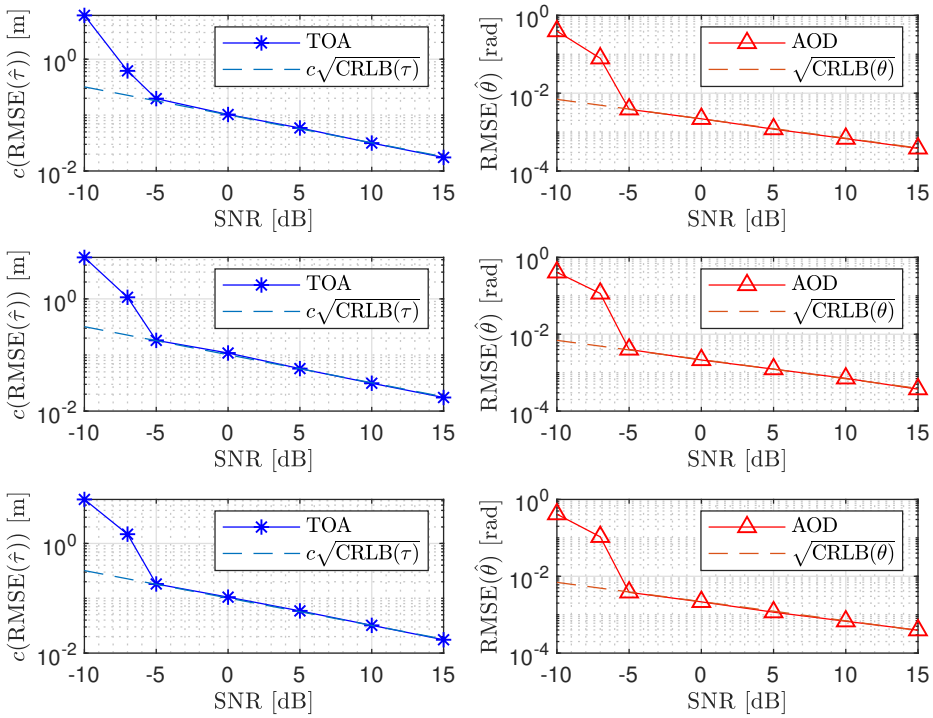

Figure 4.4: RMSEs of the estimated channel parameters $d = c\tau$ and θ for all BSs versus the CRLB for the two parameters as a function of SNR for $N_t = 40$ and $W_{\text{B}} = 100$MHz.

SNR[dB]	$\sqrt{\text{CRLB}(d)}$[cm]	RMSE$(\hat{d})$[cm]	$\sqrt{\text{CRLB}(\theta)}$[rad]	RMSE$(\hat{\theta})$[rad]
-10	32	610	6.9×10^{-3}	4.0×10^{-1}
-7	23	110	4.9×10^{-3}	1.0×10^{-1}
-5	18	19	3.9×10^{-3}	3.9×10^{-3}
0	10	11	2.2×10^{-3}	2.2×10^{-3}
5	5.7	5.9	1.2×10^{-3}	1.2×10^{-3}
10	3.2	3.2	7.0×10^{-4}	7.0×10^{-4}
15	1.8	1.8	4.0×10^{-4}	4.0×10^{-4}

Table 4.1: RMSEs of estimated channel parameters for all BSs combined and CRLB for different SNR values. With $N_t = 40$ and $W_{\text{B}} = 100$MHz.

An investigation of how frequent the distinct outliers occur show that 18 percent of the simulations at -10dB and 0.5 percent at -7dB can be considered as outliers. A distribution of the simulation results (for τ) at -10dB is presented as a histogram in Fig. 4.5 (b) compared to the theoretical PDF given by the CRLB. Most estimates are centered around zero but with a noticeable amount of outliers.

In Fig 4.6 the RMSE of the estimated positions are presented together with their corresponding PEB, calculated as in (3.17), over different SNR values. The numerical results for each SNR value are presented in Table 4.2 and shows that the

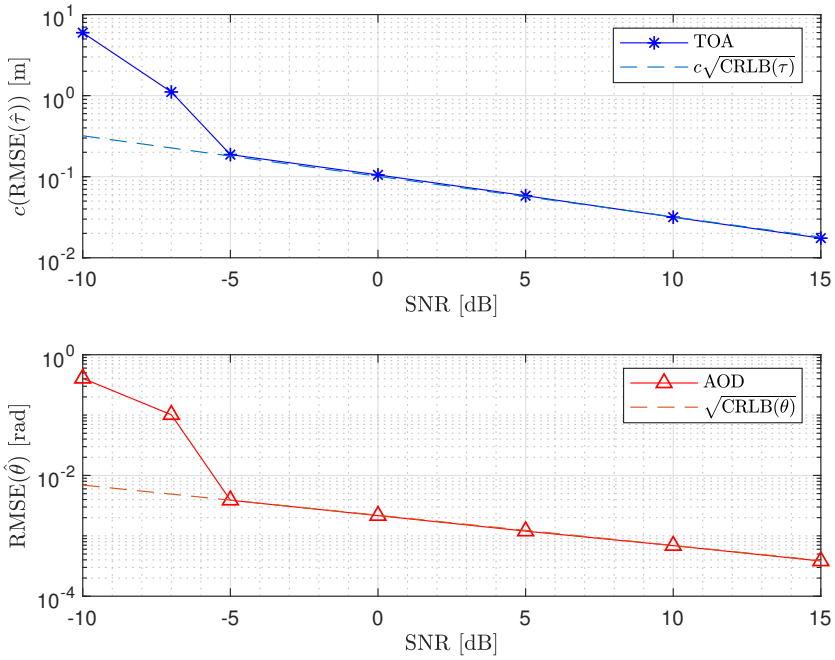

(a) RMSEs of the estimated channel parameters for all BSs combined.

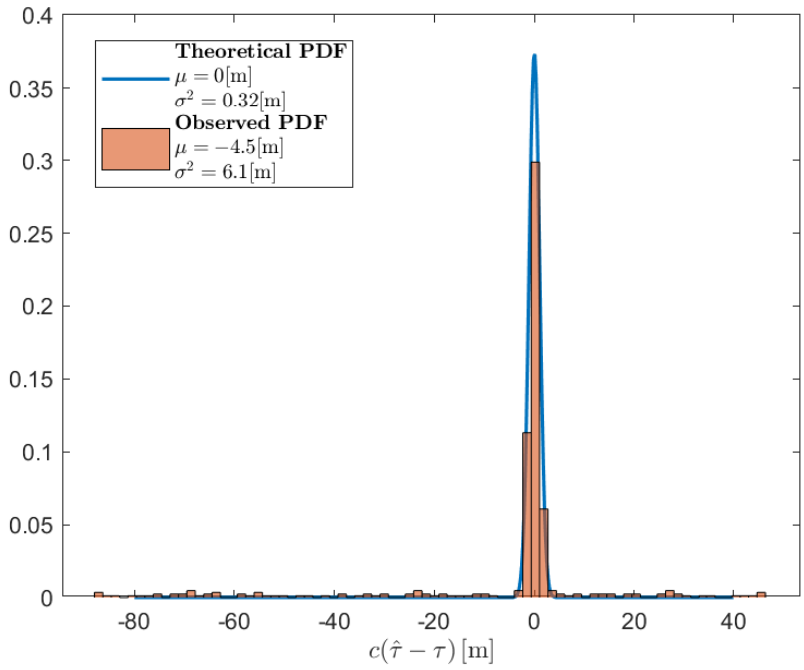

(b) Histogram of estimation errors from the estimated time delay at -10dB compared to the theoretical PDF.

Figure 4.5: Performance of the MLE versus the CRLB for varying SNR and with $N_t = 40$ and $W_\text{B} = 100$MHz.

proposed estimator achieves the PEB for SNRs from −5dB and above, even though the transformation between channel estimates and position is a non-linear conversion as described in subsection 3.3.2. Furthermore, it has greater performance than the competing individual measurement estimators and suggests that an accuracy of < 10 cm is achievable even for negative SNR vales, i.e. when the power of the noise is larger than the signal itself, and at 15dB the accuracy is around 1cm.

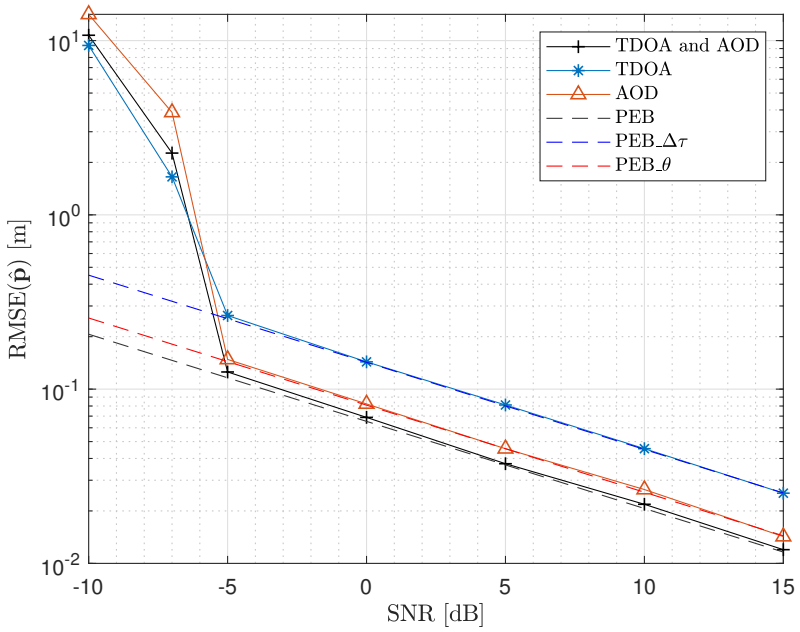

Figure 4.6: RMSEs of the position estimates $\mathbf{p}$ versus the PEB for the different estimates as a function of SNR for $N_t = 40$ and $W_{\mathrm{B}} = 100$MHz.

SNR[dB]	PEB	TDOA and AOD	$\mathrm{PEB}_{\Delta\tau}$	TDOA	PEB_{θ}	AOD
-10	21	1070	45	940	26	1410
-7	15	230	32	160	18	390
-5	12	13	25	26	14	15
0	6.5	6.9	14	14	8.1	8.2
5	3.7	3.7	8.0	8.1	4.6	4.6
10	2.1	2.2	4.5	4.6	2.6	2.7
15	1.2	1.2	2.5	2.5	1.4	1.4

Table 4.2: RMSEs [cm] of estimated position parameters and PEBs [cm] for different SNR values. With $N_t = 40$ and $W_{\mathrm{B}} = 100$MHz.

4.2.2 Scenario 2: Estimates for Varying Number of Antennas

The FIM analysis suggested that the AOD measurements was expected to be insufficient for positioning estimations at very low antenna element and with significant accuracy increase with increasing antenna elements. The results in Fig. 4.7 confirms this as the estimations improves with increasing antenna elements. The TDOA on the other hand is not significantly effected by the antennas and therefore have a more or less constant estimation accuracy. Note that with a single transmit antenna only TDOA measurements can be realized. Furthermore, Fig. 4.7 demonstrate that the channel estimator successfully reaches the CRLB for all number of antennas for both AOD and TOA.

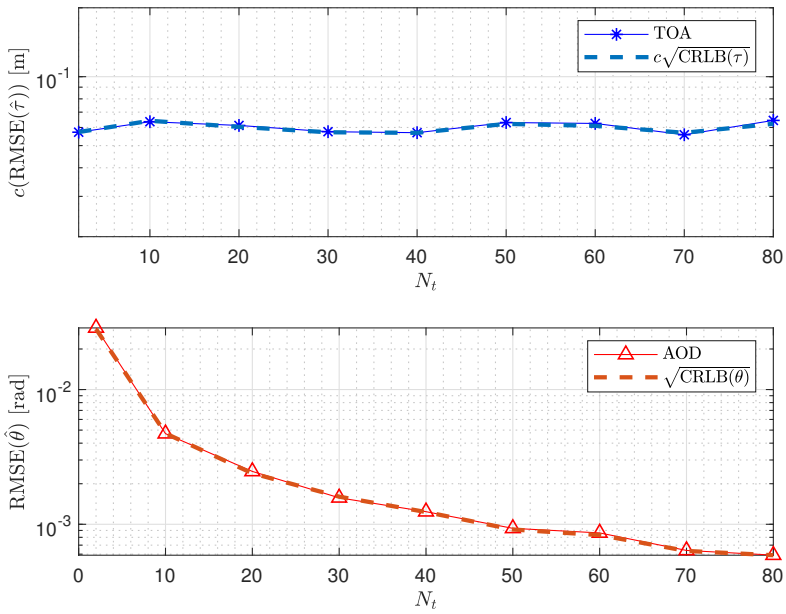

Figure 4.7: RMSEs of the estimated channel parameters $d = c\tau$ and θ for all BSs combined versus the CRLB for the two parameters as a function of antennas for SNR = 5dB and $W_{\text{B}} = 100$MHz.

In Fig. 4.8 the position estimations for varying antenna elements are presented and shows that all of the estimators are capable of reaching the PEB. The figure also demonstrate that the proposed estimator, which combines AOD and TDOA measurements perform significantly better than the estimators using only AOD or only TDOA measurements, especially between 5 and 50 antennas. Even though AOD-only performs relatively poor when the number of antennas are less than 10 the combination of both AOD and TDOA is capable of bringing the RMSE below the accuracy of TDOA-only.

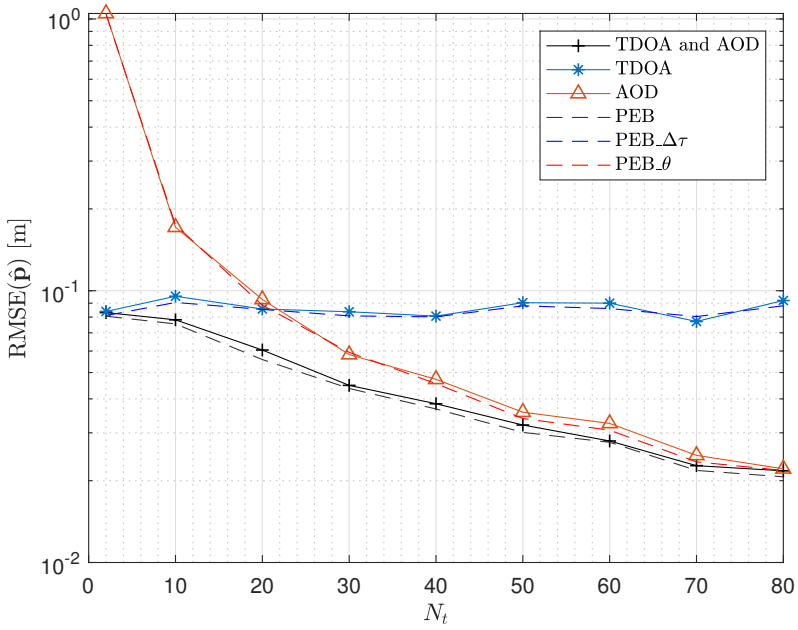

Figure 4.8: RMSEs of the position estimates $\mathbf{p}$ versus the PEB for the different estimates as a function of antennas for SNR = 5dB and $W_{\mathrm{B}} = 100$MHz.

4.2.3 Scenario 3: Estimates for Varying Bandwidth

Similarly as in the case of varying number of antennas, the FIM analysis suggested that the TOA measurements would be insufficient for accurate positioning for low bandwidths but satisfactory when the bandwidth is increased. This is again confirmed, the channel estimation results are presented in Fig. 4.9 and shows promising results as the MLE manage to attain the CRLB for both the time and angle estimates. In this scenario the TOA measurement accuracy is noticeable lower for bandwidths below 100MHz but show promising results for bandwidths $>$ 100MHz, the AOD measurements are not affected by the bandwidth. This directly reflects the position estimates presented in Fig. 4.10, the accuracy for TDOA-only significantly increases with the bandwidth while the AOD-only remains the same. The proposed estimator outperforms both the individual estimators for low bandwidths and converges to the TDOA-only estimator as the bandwidth increases.

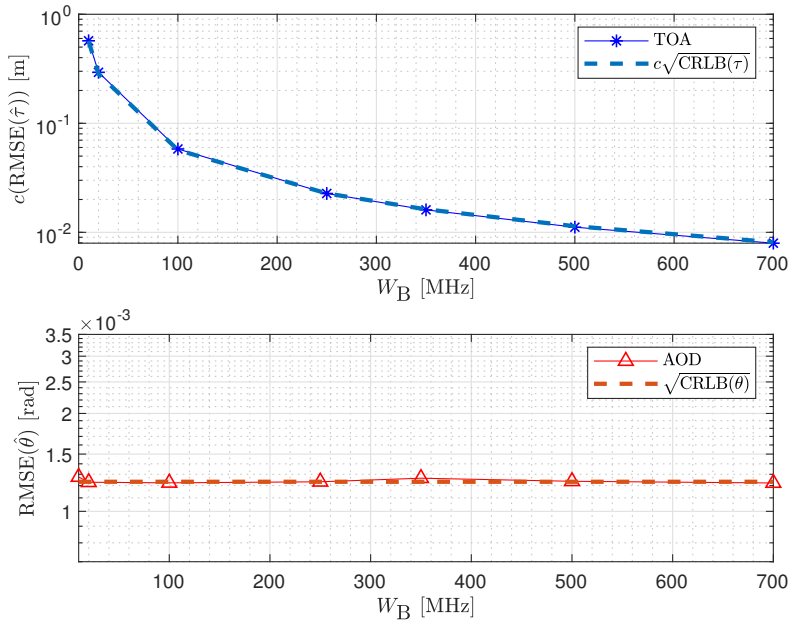

Figure 4.9: RMSEs of the estimated channel parameters $d = c\tau$ and θ for all BSs combined versus the CRLB for the two parameters as a function of bandwidth for SNR = 5dB and $N_t = 40$.

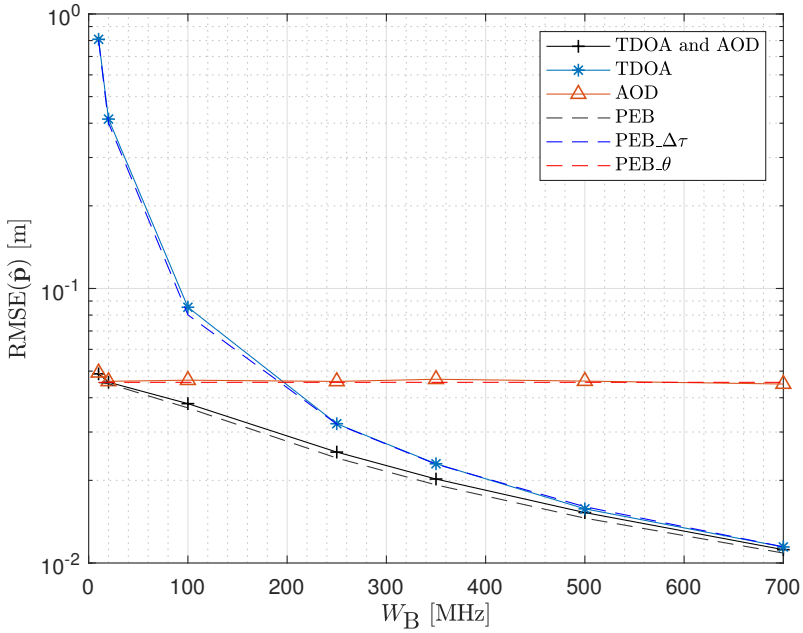

Figure 4.10: RMSEs of the position estimates $\mathbf{p}$ versus the PEB for the different estimates as a function of bandwidth for SNR = 5dB and $N_t = 40$.

5
Discussion

In this thesis we have investigated the possibility of utilizing future 5G cellular networks to determine an unknown user position. We have proposed a system model based on a wide-band mmWave MISO with an ULA structure. Assuming this model, we have investigated the possibility of determining the MS position in the DL by estimating AOD and TDOA from three synchronized BSs with a significant clock bias between the MS and the BS. Additionally, we carried out an extensive FIM analysis that provided fundamental indications of performance of different system designs, such as varying bandwidths and transmit antenna elements. The proposed estimators attains the derived theoretical performance bounds, even with low bandwidth, limited available antenna elements and for few antenna element in LOS. We saw that for SNRs around -5dB and up reaches the bounds, but fails when the SNR is below -5dB as a result of frequent outliers.

In practical implementations, where position estimators most likely have prior information of its position from previous sample instances, any outlier can be detected and discarded. Therefore, it is reasonable to conclude acceptable performance even at these low SNR values. Our proposed method of combining AOD and TDOA measurements have shown that a robust system is possible as the combination of the estimations provide redundancy in the system, especially when both AOD and TDOA measurements are sufficient. This property makes the system more flexible and less dependent on how certain 5G networks maybe be implemented. The derived FIM have proven to be a good tool that could further be studied to prepare for other variations in system design.

Results from the thesis further shows that it is possible to achieve high accuracy positioning in the DL instead of the more conventional method of computing in the UL. There are several reasons for why DL configuration is in favour of the more conventional UL configuration: A significant computational burden is eased from the BSs and user integrity is easier to maintain. Lastly, it opens up a market that allows multiple competitive companies to develop high end positioning solutions as signals in the DL are more available to everyone.

5.1 Applications

Our results from Table 4.2 suggests impressive accuracy at cm-level which indicates that it is possible to meet the necessary requirements for future autonomous vehicles that demands longitudinal and lateral positioning errors of maximum 0.29m

[46]. GNSS positioning solutions are already capable of reaching well beyond these requirements in rural areas but are facing great challenges in urban environments when no LOS is present [7]. It is very unlikely that mmWave 5G systems will be available to the entire vehicular infrastructure, but as a supplement in tunnels and urban canyons it serves as an essential part to provide full coverage. By combining high-end GNSS solutions together with a 5G localization scheme, such as we have proposed, the localization requirements for future autonomous vehicles could be reached.

A robust localization application is not only attractive from the autonomous vehicle industry but can also play an important role in other areas due to the recent expansion of location-based services. One important example of such is in emergency site localization where an emergency caller is unable to share its position and with emerging technologies such as EKG detectors in ordinary cell phones or smart watches, accurate emergency localization of an unconscious person would be critical for paramedics [47].

5.2 Future Development

The thesis have shown promising potential for a highly accurate localization system with the use of 5G. However in order for the proposed estimator to be implemented, further developments of this thesis are required. Our method is based on a mathematical model and will obviously differ from real-life scenarios and hardware setups. An extensive study on how well these models match a hardware setup is paramount for practical implementations. In this thesis we considered a scenario with a strong LOS signal and without NLOS or OLOS signals present which is highly unrealistic in a real-life scenario, where multiple paths are almost inevitable. The system model and estimators would therefore need certain extensions to cover more possible scenarios with NLOS and OLOS components included.

In order to realize a localization service, our stationary case study needs to be extended by including a dynamic model. Since moving objects would give rise to frequency shifts of the signal (Doppler effect [31]) the system model in section 2.1 would need to be further supplemented with a model that encapsulates this phenomenon. This would give rise to a third dimensional estimation problem and thus increasing the computational burden of the estimation process where the Doppler estimation is included. To ease the burden, the proposed algorithm could be combined with a nonlinear estimator, e.g. a particle filter or an extended Kalman filter that makes use of the previous estimation mean and covariance to predict the forthcoming estimations [48]. This would decrease the computational burden as the probable search areas becomes significantly smaller.

Our study shows that the azimuth AOD can be estimated with great precision, however if an elevation angle is required an extended antenna modulation model is needed. In such scenario it is required that the BSs are equipped with planar array structures such as a Uniform Rectangular Array (URA). In later phases of 5G

development it is most likely that MS will be equipped with large antenna arrays as well, this would imply that also AOA could be estimated, which would increase the robustness of the system and potentially increase the positioning accuracy.

6
Conclusions

In this thesis, a model of a wide band mm-Wave MISO system has been derived as an attempt to mimic a future potential 5G system. Based on this model, the problem of determining a single receiver antenna MS position, in presence of a synchronization bias and with multiple BSs, was investigated. From an extensive Fisher information analysis, theoretical lower bounds on the estimation performance was derived. The results from the analysis demonstrates great potential in positioning estimation and shows that cm-level accuracy is possible. In an attempt to reach these bounds, a low-complexity two-step algorithm was proposed. The estimator uses a combination of TOA and AOD measurements by solving a two-dimensional ML problem. To account for the present clock bias, TDOA measurements were computed and together with the AOD measurements in a weighted LS estimator, the MS position was estimated. Based on 500 MC simulations it is demonstrated that the proposed algorithm is capable of attaining the theoretical lower bounds and outperforms AOD-only and TDOA-only estimators even when bandwidth is limited or in the case of few transmit antennas.

Bibliography

[1] M. van Ratingen, A. Williams, A. Lie, A. Seeck, P. Castaing, R. Kolke, G. Adriaenssens, and A. Miller, "The european new car assessment programme: A historical review," *Chinese Journal of Traumatology*, vol. 19, no. 2, pp. 63 – 69, 2016.

[2] I. American Automobile Association, "Advanced driver assistance technology names," 2019.

[3] A. J. Benson, B. C. Tefft, A. M. Svancara, and W. J. Horrey, "Potential reductions in crashes, injuries, and deaths from large-scale deployment of advanced driver assistance systems (research brief)," *AAA Foundation for Traffic Safety*, 2018.

[4] S. Kuutti, S. Fallah, K. Katsaros, M. Dianati, F. Mccullough, and A. Mouzakitis, "A survey of the state-of-the-art localization techniques and their potentials for autonomous vehicle applications," *IEEE Internet of Things Journal*, vol. 5, pp. 829–846, April 2018.

[5] M. Klomp, M. Jonasson, L. Laine, L. Henderson, E. Regolin, and S. Schumi, "Trends in vehicle motion control for automated driving on public roads," *Vehicle System Dynamics*, vol. 57, no. 7, pp. 1028–1061, 2019.

[6] H. Seif and X. Hu, "Autonomous driving in the icity—hd maps as a key challenge of the automotive industry," *Engineering*, vol. 2, pp. 159–162, 06 2016.

[7] J. A. del Peral-Rosado, R. Raulefs, J. A. López-Salcedo, and G. Seco-Granados, "Survey of cellular mobile radio localization methods: From 1g to 5g," *IEEE Communications Surveys Tutorials*, vol. 20, pp. 1124–1148, Secondquarter 2018.

[8] P. D. Groves and Z. Jiang, "Height aiding, c/n0 weighting and consistency checking for gnss nlos and multipath mitigation in urban areas," *Journal of Navigation*, vol. 66, no. 5, p. 653–669, 2013.

[9] A. Fascista, A. Coluccia, H. Wymeersch, and G. Seco-Granados, "Millimeter-wave downlink positioning with a single-antenna receiver," *IEEE Transactions on Wireless Communications*, vol. 18, pp. 4479–4490, Sep. 2019.

[10] A. Shahmansoori, G. Garcia, G. Destino, G. Seco-Granados, and H. Wymeersch, "Position and orientation estimation through millimeter-wave mimo in 5G systems," *IEEE Transactions on Wireless Communications*, vol. 17, pp. 1822–1835, March 2018.

[11] H. Wymeersch, U. Ferner, and M. Z. Win, "Cooperative bayesian self-tracking for wireless networks," *IEEE Communications Letters*, vol. 12, pp. 505–507, July 2008.

[12] G. Rodrigues de Campos, P. Falcone, R. Hult, H. Wymeersch, and J. Sjöberg, "Traffic coordination at road intersections: Autonomous decision-making algorithms using model-based heuristics," *IEEE Intelligent Transportation Systems Magazine*, vol. 9, pp. 8–21, Spring 2017.

[13] R. Mardeni, P. Shahabi, and M. Riahimanesh, "Mobile station localization in wireless cellular systems using UTDOA," in *2012 International Conference on Microwave and Millimeter Wave Technology (ICMMT)*, vol. 5, pp. 1–4, May 2012.

[14] J. Liu and S. Feng, "Enhanced RSTD for scalable bandwidth of OTDOA positioning in 3GPP LTE," in *2013 International Conference on Localization and GNSS (ICL-GNSS)*, pp. 1–5, June 2013.

[15] Y. Sun, K. C. Ho, and Q. Wan, "Solution and analysis of TDOA localization of a near or distant source in closed form," *IEEE Transactions on Signal Processing*, vol. 67, pp. 320–335, Jan 2019.

[16] J. J. Caffery and G. L. Stuber, "Overview of radiolocation in CDMA cellular systems," *IEEE Communications Magazine*, vol. 36, pp. 38–45, April 1998.

[17] K. Cheung, H. So, W.-K. Ma, and Y. Chan, "A constrained least squares approach to mobile positioning: Algorithms and optimality," *EURASIP Journal on Advances in Signal Processing*, vol. 2006, p. 020858, Dec 2006.

[18] S. Kong and B. Kim, "Error analysis of the OTDOA from the resolved first arrival path in LTE," *IEEE Transactions on Wireless Communications*, vol. 15, pp. 6598–6610, Oct 2016.

[19] F. Gustafsson and F. Gunnarsson, "Mobile positioning using wireless networks: possibilities and fundamental limitations based on available wireless network measurements," *IEEE Signal Processing Magazine*, vol. 22, pp. 41–53, July 2005.

[20] L. Cong and W. Zhuang, "Hybrid TDOA/AOA mobile user location for wideband CDMA cellular systems," *IEEE Transactions on Wireless Communications*, vol. 1, pp. 439–447, July 2002.

[21] N. J. Thomas, D. G. M. Cruickshank, and D. I. Laurenson, "Performance of a TDOA-AOA hybrid mobile location system," in *Second International Conference on 3G Mobile Communication Technologies*, pp. 216–220, March 2001.

[22] Z. Abu-Shaban, X. Zhou, T. Abhayapala, G. Seco-Granados, and H. Wymeersch, "Error bounds for uplink and downlink 3D localization in 5G millimeter wave systems," *IEEE Transactions on Wireless Communications*, vol. 17, pp. 4939–4954, Aug 2018.

[23] Geneva: World Health Organization, "Global status report on road safety 2018," *Licence: CC BYNC-SA 3.0*, (2018).

[24] K. A. Brookhuis, D. de Waard, and W. H. Janssen, "Behavioural impacts of advanced driver assistance systems–an overview," *European Journal of Transport and Infrastructure Research*, (2019).

[25] H. A. Najada and I. Mahgoub, "Autonomous vehicles safe-optimal trajectory selection based on big data analysis and predefined user preferences," in *2016 IEEE 7th Annual Ubiquitous Computing, Electronics Mobile Communication Conference (UEMCON)*, pp. 1–6, Oct 2016.

[26] N. Zhu, J. Marais, D. Bétaille, and M. Berbineau, "GNSS position integrity in urban environments: A review of literature," *IEEE Transactions on Intelligent Transportation Systems*, vol. 19, pp. 2762–2778, Sep. 2018.

[27] K. Alharbi and X. Lin, "Efficient and privacy-preserving smart grid downlink communication using identity based signcryption," in *2016 IEEE Global Communications Conference (GLOBECOM)*, pp. 1–6, Dec 2016.

[28] A. Goldsmith, "Multicarrier modulation," in *Wireless Communications*, pp. 374–397, Cambridge University Press, 2005.

[29] C. Balanis, *Introduction to Smart Antennas*. Morgan and Claypool Publishers, 1st ed., 2007.

[30] T. Tjelta, "Euro-5G – supporting the european 5G initiative," 2017.

[31] A. Goldsmith, "Statistical multipath channel models," in *Wireless Communications*, pp. 64–94, Cambridge University Press, 2005.

[32] C. Balanis, *Introduction to Smart Antennas*. Morgan and Claypool Publishers, 1st ed., 2007.

[33] F. Gustafsson and F. Gunnarsson, "Mobile positioning using wireless networks: possibilities and fundamental limitations based on available wireless network measurements," *IEEE Signal Processing Magazine*, vol. 22, pp. 41–53, July 2005.

[34] S. Gleason and D. Gebre-Egziabher, "Combining GNSS with RF systems," in *GNSS Applications and Methods*, pp. 211–244, Artech House, 2009.

[35] L. Jaulin, "5 - instantaneous localization," in *Mobile Robotics* (L. Jaulin, ed.), pp. 171 – 196, Elsevier, 2015.

[36] C. Zhizhang, G. K. Gokeda, and Y. Yu, *Introduction to Direction-of-Arrival Estimation*. Artech House, 1 ed., 2010.

[37] B. Efron, "Defining the curvature of a statistical problem (with applications to second order efficiency)," *Ann. Statist.*, vol. 3, pp. 1189–1242, 11 1975.

[38] A. Ly, M. Marsman, J. Verhagen, R. Grasman, and E.-J. Wagenmakers, "A tutorial on fisher information," 2017.

[39] S. M. Kay, *Fundamentals of Statistical Signal Processing: Estimation Theory*. Prentice Hall, 1997.

[40] M. Stein, J. A. Nossek, and K. Barbé, "Fisher information lower bounds with applications in hardware-aware nonlinear signal processing," 2015.

[41] Y. Wang, D. Tian, Z. Sheng, and W. Jian, *Connected Vehicle Systems: Communication, Data, and Control*. USA: CRC Press, Inc., 1st ed., 2017.

[42] S. Miller and D. Childers, "Complex random variables," in *Probability and Random Processes*, pp. 267–270, Elsevier, 2012.

[43] S. Miller and D. Childers, "Random processes in linear systems," in *Probability and Random Processes*, pp. 473–515, Elsevier, 2012.

[44] S. Miller and D. Childers, "Complex random variables," in *Probability and Random Processes*, pp. 219–221, Elsevier, 2012.

[45] A. Thode, M. Zanolin, E. Naftali, I. Ingram, P. Ratilal, and N. C. Makris, "Necessary conditions for a maximum likelihood estimate to become asymptotically unbiased and attain the cramer–rao lower bound. ii. range and depth localization of a sound source in an ocean waveguide," *The Journal of the Acoustical Society of America*, vol. 112, no. 5, pp. 1890–1910, 2002.

[46] T. G. Reid, S. E. Houts, R. Cammarata, G. Mills, S. Agarwal, A. Vora, and G. Pandey, "Localization requirements for autonomous vehicles," *SAE International Journal of Connected and Automated Vehicles*, vol. 2, Sep 2019.

[47] J. Wasserlauf, C. You, R. Patel, A. Valys, D. Albert, and R. Passman, "Smartwatch performance for the detection and quantification of atrial fibrillation," *Circulation: Arrhythmia and Electrophysiology*, vol. 12, no. 6, p. e006834, 2019.

[48] S. Särkkä, *Bayesian filtering and smoothing.* Cambridge University Press, 2013.

A

Appendix A

FIM for position with TOA-only measurements

Consider the channel parameter vector

$$\tilde{\boldsymbol{\zeta}}_i = [\rho_i, \phi_i, \tau_i]^T, i = 1, \ldots, N_{\mathrm{BS}}. \tag{A.1}$$

The channel FIM $\mathbf{I}_{\boldsymbol{\zeta}_i}$ (3.3) was modified to exclude the information from the AOD parameter

$$\mathbf{I}_{\tilde{\boldsymbol{\zeta}}_i} = \left[\mathbf{I}_{\boldsymbol{\zeta}_i}\right]_{1:3,1:3}. \tag{A.2}$$

The Jacobian transformation is defined in (3.8) and with (A.2) it was calculated as

$$\tilde{\mathbf{I}}_{\eta_i} = \tilde{\mathbf{T}}_i^{\mathrm{T}} \mathbf{I}_{\tilde{\zeta}_i} \tilde{\mathbf{T}}_i, \tag{A.3}$$

where the transformation matrix was defined as

$$\tilde{\mathbf{T}}_i \overset{\text{def}}{=} \frac{\partial \tilde{\boldsymbol{\zeta}}_i^{\mathrm{T}}}{\partial \boldsymbol{\eta}_i} \begin{bmatrix} \partial\rho_i/\partial\rho_i & \partial\rho_i/\partial\phi_i & \partial\rho_i/\partial\mathbf{p} & \partial\rho_i/\partial b \\ \partial\phi_i/\partial\rho_i & \partial\phi_i/\partial\phi_i & \partial\phi_i/\partial\mathbf{p} & \partial\phi_i/\partial b \\ \partial\tau_i/\partial\rho_i & \partial\tau_i/\partial\phi_i & \partial\tau_i/\partial\mathbf{p} & \partial\tau_i/\partial b \end{bmatrix} = \begin{bmatrix} 1 & 0 & 0 & 0 \\ 0 & 1 & 0 & 0 \\ 0 & 0 & \partial\tau_i/\partial\mathbf{p} & \partial\tau_i/\partial b \end{bmatrix}. \tag{A.4}$$

By recalling that τ_i (2.4) is a geometric function of $\mathbf{p}$, the corresponding derivatives was defined in (3.10) and (3.12). The result of the transformation is a 5×5 always singular matrix. The rest of the calculations to derive the EFIM for position with TOA-only measurements are the same as in (3.13) - (3.16) with $\tilde{\mathbf{I}}_{\eta_i}$ as the position FIM.

FIM for position with AOD-only measurements

Consider the channel parameter vector

$$\bar{\boldsymbol{\zeta}}_i = [\rho_i, \phi_i, \theta_i]^T. \tag{A.5}$$

The channel FIM $\mathbf{I}_{\boldsymbol{\zeta}_i}$ (3.3) was modified to exclude the information from the TOA parameter, in a similar way as in (A.2). The result is the modified channel FIM $\mathbf{I}_{\bar{\boldsymbol{\zeta}}_i}$. The Jacobian transformation of $\mathbf{I}_{\bar{\boldsymbol{\zeta}}_i}$ with position parameter vector $\bar{\boldsymbol{\eta}}_i = \left[\rho_i, \phi_i, \mathbf{p}^T\right]^T$ was calculated as

$$\bar{\mathbf{I}}_{\eta_i} = \bar{\mathbf{T}}_i^{\mathrm{T}} \mathbf{I}_{\bar{\zeta}_i} \bar{\mathbf{T}}_i, \tag{A.6}$$

with the transformation matrix

$$\bar{\mathbf{T}}_i \overset{\text{def}}{=} \frac{\partial \bar{\boldsymbol{\zeta}}_i^{\mathrm{T}}}{\partial \boldsymbol{\eta}_i} \begin{bmatrix} \partial\rho_i/\partial\rho_i & \partial\rho_i/\partial\phi_i & \partial\rho_i/\partial\mathbf{p} \\ \partial\phi_i/\partial\rho_i & \partial\phi_i/\partial\phi_i & \partial\phi_i/\partial\mathbf{p} \\ \partial\theta_i/\partial\rho_i & \partial\theta_i/\partial\phi_i & \partial\theta_i/\partial\mathbf{p} \end{bmatrix} = \begin{bmatrix} 1 & 0 & 0 \\ 0 & 1 & 0 \\ 0 & 0 & \partial\theta_i/\partial\mathbf{p} \end{bmatrix}. \tag{A.7}$$

By recalling that θ_i (2.8) is a geometric function of $\mathbf{p}$, the corresponding derivative was defined in (3.11). The result of the transformation is a 4×4 non-singular matrix. It is still of interest to construct the collective FIM as in (3.15) in order to receive the information from all BSs, with the collective position parameter vector $\bar{\boldsymbol{\eta}} = \left[\rho_1, \dots \rho_{N_{\mathrm{BS}}}, \phi_1, \dots, \phi_{N_{\mathrm{BS}}}, \mathbf{p}^T\right]^T$. The decomposition in (3.13) was used and since no bias emerges in the transformation the following matrices were redefined as $\mathbf{B}_i \in \mathbb{R}^{2\times 2}$ and $\mathbf{C}_i \in \mathbb{R}^{2\times 2}$. Finally, the EFIM for position with AOD-only measurements with respect to $\boldsymbol{\pi} = \mathbf{p}^T$ was found by applying (3.16).

B

Appendix B

Position estimates with TDOA-only measurements

Consider the observation vector from chapter 3 in (3.28) but with AOD estimations excluded

$$\hat{\tilde{\boldsymbol{\psi}}} = [\Delta\hat{\tau}_1, \ldots, \Delta\hat{\tau}_{N_{\mathrm{BS}}-1}]^{\mathrm{T}} \in \mathbb{R}^{(N_{\mathrm{BS}}-1)\times 1} \tag{B.1}$$

and further the time geometric function of $\mathbf{p}$ as in (2.4) but without the bias term. The time difference was further expressed as a function of $\mathbf{p}$, with BS $i = N_{\mathrm{BS}}$ as the chosen reference station

$$\tilde{f}(\mathbf{p}) = \begin{bmatrix} \Delta\hat{\tau}_1(\mathbf{p}) \\ \vdots \\ \Delta\hat{\tau}_{N_{\mathrm{BS}}-1}(\mathbf{p}) \end{bmatrix} = \frac{1}{c} \begin{bmatrix} \|\mathbf{p} - \mathbf{p}_1\| - \|\mathbf{p} - \mathbf{p}_{N_{BS}}\| \\ \vdots \\ \|\mathbf{p} - \mathbf{p}_{N_{\mathrm{BS}}-1}\| - \|\mathbf{p} - \mathbf{p}_{N_{BS}}\| \end{bmatrix} \in \mathbb{R}^{(N_{\mathrm{BS}}-1)\times 1}. \tag{B.2}$$

The position estimates, when only considering TDOA measurements can readily be found by solving the LS problem in (3.30) with $\hat{\tilde{\boldsymbol{\psi}}}$ and $\tilde{f}(\mathbf{p})$ as above and with $\boldsymbol{\Sigma}^{-1}$ as described in subsection 3.3.2.

Position estimates with AOD-only measurements

With the same reasoning as above, consider (3.28) but with TDOA estimations excluded

$$\hat{\bar{\boldsymbol{\psi}}} = [\hat{\theta}_1, \ldots, \hat{\theta}_{N_{\mathrm{BS}}}]^{\mathrm{T}} \in \mathbb{R}^{N_{\mathrm{BS}}\times 1} \tag{B.3}$$

and further the angle geometric function of $\mathbf{p}$ as in (2.8)

$$\bar{f}(\mathbf{p}) = \begin{bmatrix} \hat{\theta}_1(\mathbf{p}) \\ \vdots \\ \hat{\theta}_{N_{\mathrm{BS}}}(\mathbf{p}) \end{bmatrix} = \begin{bmatrix} \operatorname{atan2}(p_y - y_1, p_x - x_1) \\ \vdots \\ \operatorname{atan2}(p_y - y_{N_{\mathrm{BS}}}, p_x - x_{N_{\mathrm{BS}}}) \end{bmatrix} \in \mathbb{R}^{N_{\mathrm{BS}}\times 1} \tag{B.4}$$

The position estimates, when only considering AOD measurements can readily be found by solving the LS problem in (3.30) with $\hat{\bar{\boldsymbol{\psi}}}$ and $\bar{f}(\mathbf{p})$ as above and with $\boldsymbol{\Sigma}^{-1}$ as described in subsection 3.3.2.